



1

2 **Assessing Terrestrial Water Storage Change Since the**
3 **1980s**

4

5 Franklin R. Robertson¹, Michael G. Bosilovich², Matthew Rodell², Richard P. Allan³,

6 Bryant Loomis², Hiroko Beaudoin^{2,4}, Joaquín Muñoz-Sabater⁵ and Jason B. Roberts¹

7

8 ¹Earth System Science Center, University of Alabama in Huntsville, Huntsville, AL 35805

9 ²NASA / Goddard Space Flight Center, Greenbelt, MD 20771

10 ³Department of Meteorology and National Centre for Earth Observation, University of Reading,

11 Reading, RG6 6UR, UK

12 ⁴Earth System Science Interdisciplinary Center, University of Maryland, College Park, College

13 Park, MD

14 ⁵European Centre for Medium-Range Weather Forecasts, Bonn, Germany

15 *Correspondence to:* Franklin R. Robertson (fr0003@uah.edu, pete.robertson@nasa.gov)

16

17 ***Abstract***

18 Water availability for societies and ecosystems depends upon Terrestrial Water Storage (TWS),
19 yet global, spatially resolved measurements are largely unavailable before the advent of the
20 Gravity Recovery and Climate Experiment (GRACE) gravimetric measurements in 2002. By
21 exploiting a larger set of model and observations-based datasets than previously considered, along
22 with statistical and machine learning techniques, we advance understanding of TWS changes since
23 the 1980s, including accounting for human water management (HWM).



24 A decline in TWS during 2002-2019 is identified for three global hydrologic models with HWM
25 and bias-corrected precipitation forcing (-0.91 to -0.06 mm yr⁻¹) with only one showing larger
26 decreases than observed by GRACE observations (-0.80 mm y⁻¹). We further identify a longer-
27 term decline in TWS during 1980-2019 in these models, linked with regional precipitation
28 decreases and the net effects of HWM through TWS drawdowns over northern India, southwest
29 U.S. and northeastern China, yet the amplitude of the global land trends remains poorly quantified,
30 ranging from -0.72 to $+0.04$ mm y⁻¹. Statistical / Machine Learning (ML) reconstructions are found
31 to match GRACE variability but their fidelity in the pre-GRACE/FO period remains unknown.

32 A stronger decline in TWS since 1980 in the European Centre for Medium-range Weather
33 Forecasts 5th generation reanalysis (ERA5) enhanced land component (ERA5-Land) is linked to
34 an artificial drop in precipitation around 2000-2002 in ERA5 that is most pronounced over
35 equatorial central Africa, northeastern China and the northern Argentina / La Plata region. Our
36 findings urge caution in inferring changes in hydroclimate variables from ERA5-Land and other
37 reanalyses due to inhomogeneities in the assimilated observational data. Continued emphasis on
38 bias corrections to hydrometeorological data and better modeling of HWM are crucial to
39 improving all retrospective analyses of changes in land surface hydrology and terrestrial water
40 stores.

41

42 **1 Introduction**

43 The global distribution and temporal evolution of Terrestrial Water Storage (TWS)¹ have profound
44 consequences for human society. Access to water for irrigation, human health (consumption,
45 sanitation), power generation, manufacturing, sustainable development and a supply resilient to
46 climate change each demand improved assays of historical water distribution, availability and
47 projections for the future (Vorosmarty et al, 2000; Wada and Bierkens, 2014; Rodell et al, 2018;
48 Deng et al, 2025). TWS is also physically linked to freshwater discharge to the global oceans and,
49 thus, Global Mean Sea-Level (GMSL) change (Pokhrel et al, 2012; Boening et al, 2012; Wada et
50 al, 2017; Rodell et al, 2024; Chandanpurkar et al, 2025). TWS evolves as the net effect of
51 precipitation (P), evapotranspiration (ET), runoff or discharge (RO), and the collection of human

¹ Appendix A contains a full list of acronyms



52 influences we refer to here as Human Water Management (HWM). In a stationary climate,
53 changes in TWS would largely vanish annually; this assumption, valid to first order on multi-
54 annual timescales, has underpinned the success of Budyko's (1974) relationships in analyzing
55 hydrologic behavior over differing climate regimes. But with significant natural climate
56 variability, changing climate forcing that alters near-surface hydrometeorology, as well as the
57 related growth of human activities altering vegetation, land, and water use, TWS variations and
58 trends constitute important but poorly determined parts of the evolving terrestrial water balance.

59 Strategies for measuring TWS and its change have improved radically in recent decades. Satellite
60 LASER Ranging (SLR) sensors provided the first spaceborne measurements of gravity changes at
61 global and continental scale extending back to 1993 (Sośnica et al, 2015; Löcher and Kusche,
62 2020; Flechtner et al., 2021; Rodell et al, 2024; Nie et al, 2025); however, the coarse spatial
63 resolution and larger uncertainties early in the period present notable limitations. GRACE
64 (NASA's Gravity Recovery and Climate Experiment, Tapley et al., 2019) and its follow-on
65 satellite mission GRACE-FO (Landerer et al., 2020), hereafter referred together as GRACE/FO,
66 have provided the first regionally detailed measurements of water mass changes over land, ocean,
67 ice sheets, and glaciers since early 2002. Advances in detailing TWS changes since that date
68 (Rodell and Reager, 2023) have enabled much greater precision in quantifying the components of
69 climate variability (Boening et al, 2012; Phillips et al, 2012; Ni et al, 2018; Tapley et al., 2019),
70 irrigation and groundwater depletion (Rodell et al, 2009; Adams et al., 2022; Scanlon et al, 2023;
71 Dharpure et al, 2025), and warming-induced cryospheric mass loss (Jacob et al., 2012; Velicogna
72 et al., 2014, 2020; Loomis et al., 2019b). Quantifying these contributing processes has provided a
73 valuable measurement and understanding of the mass related component of GMSL change,
74 complementary to the altimetric measurements of total sea level rise that also includes thermal
75 expansion of warmer oceans (Church et al., 2013).

76 The societal dependence on water availability demands a larger historical context for TWS changes
77 that extends into the decades before space-based gravimetry. Numerical models, which differ in
78 terms of the physical and biogeochemical processes and human interventions they emphasize, are
79 valuable tools for inferring TWS behavior prior to the GRACE/FO era. Bierkens (2015) offered a
80 genealogy of the various approaches, identifying four types: (i) Land Surface Models (LSMs) that
81 emphasize energy and water exchange at the soil-vegetation-atmosphere interface, (ii) Land Earth



82 System Models (LESMs) that typically include plant phenology and carbon cycling in addition to
83 more in-depth hydrology, (iii) Dynamic Vegetation Models (DVMs) that emphasize biome
84 evolution, but typically at the expense of hydrologic rigor, and (iv) Global Hydrology and Water
85 Resource Models (GHMs) that incorporate water use and which may be constrained by
86 measurements of HWM. Of course, these boundaries are not rigid. In the present analysis we will
87 include models from each of these categories. One approach to extending the TWS record has
88 been the use of offline versions of these global models driven with historical meteorological and
89 radiative forcing data (e.g., Rodell et al., 2004; Sheffield and Wood, 2007; Li et al., 2019; Cáceres
90 et al., 2020), or similar products taken from global atmospheric reanalyses (Reichle et al., 2012;
91 Muñoz-Sabater et al., 2021). A commonality of these efforts is that the results are sensitive to the
92 accuracy of meteorological forcing, model parameters, assumed soil and vegetation characteristics,
93 and uncertainties in water resource data. (Wheedon et al., 2011, 2014).

94 Another approach to inferring past TWS changes differs fundamentally from physical modeling
95 in that it involves various statistical techniques such as regression, principal component analysis
96 or machine learning (ML) which are used to replicate the GRACE/FO TWS record and then to
97 extend these empirically based estimates back prior to 2002. Among these efforts are data sets
98 produced by Humphrey and Gudmundsson, (2019), Li et al. (2021), Chandanpurkar et al. (2022)
99 and Yin et al. (2023). Some initial assessments of their accuracy are becoming available (Deng et
100 al, 2023; Hacker and Kusche, 2024). As with the physical models, the accuracy of input training
101 data is crucial with precipitation being of primary importance.

102 In this study we offer a benchmark of current capabilities in estimating TWS changes in the two
103 decades before GRACE launched, focusing particularly on trends and interannual variations over
104 the satellite era, nominally 1980 to near present. GRACE/FO retrievals of TWS are available only
105 from 2002 onward, but they constitute an important tool to judge the various TWS estimates after
106 that date, specifically in replicating pattern structure and amplitude. Our analysis centers
107 primarily, but not exclusively, on the behavior of the ERA5-Land reanalysis (Muñoz-Sabater et
108 al., 2021) because it supports a substantial fraction of land surface hydrology studies and serves as
109 a key input to many TWS reanalyses and reconstructions. It relies on the ERA5 atmospheric
110 reanalyses and thus, like other reanalyses, is subject to time dependent biases induced by
111 assimilation of an ever changing mix of observing systems, most critically, the discrete sequence



112 of satellite system changes. Further, the consequences of such biases on ERA5-Land are likely to
113 be mirrored in other ERA5 driven reanalyses. In particular, number of investigations have noted
114 likely artifacts in ERA5's hydrologic cycle stemming from these assimilation issues (Hersbach et
115 al., 2019; Nogueira et al., 2020; Gleixner et al., 2020; Cleeland et al., 2024; Rodell et al., 2024;
116 Wang et al., 2026). We review results from a number of GHM and LSM modeling efforts from
117 the Inter-Sectoral Impact Model Inter-comparison Project, ISIMIP3a (Gosling et al., 2025) whose
118 atmospheric forcing, including precipitation, benefits from attempts to reduce time-dependent
119 biases. HWM contributions in three different ISIMIP3a models are considered, contrasting their
120 TWS variations with those of ISIMIP3a LSMs that don't account for these effects. A surprising
121 result, given that ERA5-Land does not account for HWM, is that downward TWS trends from
122 ERA5-Land over the 1980-2019 period are as large or larger than those of the two GHMs. Given
123 that the ERA5-Land formulation is essentially an LESM, we investigate the potential role of
124 differences in forcing datasets used by ERA5-Land and ISIMIP3a models, principally the
125 precipitation forcing. The additional perspective of three statistical TWS reconstructions is also
126 considered as we compare their trend patterns and interannual signals to modeling results, ERA5-
127 Land behavior and to GRACE/FO. Our analysis addresses global mean trends and variability but
128 we also examine regional patterns of TWS and P that comprise global values.

129 **2 Methods and Data Sets**

130 This study uses six types of data in monthly mean, gridded form: (i) the ERA5-Land reanalysis,
131 (ii) TWS retrievals from GRACE/FO, (iii) Global Satellite LASER Ranging (SLR) based TWS
132 estimates, (iv) Model data including input precipitation and output TWS from the Inter-Sectoral
133 Impact Model Inter-comparison Project, ISIMIP3a (Warszawski et al., 2013), (v) Three statistical
134 TWS reconstructions based on training hydrometeorological predictors on the GRACE/FO record,
135 and (vi) Gridded precipitation data sets from the Global Precipitation Climatology Centre (GPCC),
136 the Global Precipitation Climatology Project, GPCP v3.2, and CRUJRA 2.2, a gridded time series
137 meteorological variables produced by the Climatic Research Unit (CRU) at the University of East
138 Anglia (UEA) (<https://catalogue.ceda.ac.uk/uuid/10d2c73e5a7d46f4ada08b0a26302ef7>).

139 **2.1 ERA5-Land**



140 ERA5-Land (Muñoz-Sabater et al., 2021) is a continuing land surface reanalysis describing the
141 water and energy balance globally at 9km daily resolution covering the period 1950 to near present.
142 The assimilating model is the Carbon Hydrology-Tiled Scheme for Surface Exchanges over Land
143 (CHTESSEL; Boussetta et al., 2021). In its ERA5-Land configuration there are four soil layers
144 (7, 21, 72 and 189 cm thick) with a total depth of 2.89m. Recent improvements to CHTESSEL
145 include incorporation of dynamic vegetation, an updated snow scheme, treatment of lake fractions,
146 and treatment of urban land attributes. ERA5-Land was produced in separate, overlapping streams
147 starting in 2001 and streams 2 and 3 initiated in 1980 and 1950. Three years of spin-up was used
148 in the overlap period. ERA5-Land is driven by hourly ERA5 atmospheric reanalysis near surface
149 meteorology, radiation and precipitation. One notable aspect of the surface evaporation
150 calculation is that potential evapotranspiration is calculated assuming crop-type vegetation with
151 no moisture stress but that the overlying atmosphere is not affected by this artificial surface
152 condition.

153

154 **2.2. GRACE and GRACE-FO**

155 GRACE (2002-2017) and GRACE-FO (2018-present) are twin satellite systems that infer time
156 varying mass distributions over the globe based on precise measurements of intersatellite range
157 (distance). These systems resolve gravity variations due to various geophysical processes, among
158 them being changes in liquid and frozen water on and under the land surface. We use an average
159 of three different Level III liquid water equivalent GRACE solutions, each at 0.5 degree resolution:
160 (i) the GSFC mass concentration blocks (mascons) product
161 GSFC.glb.200204_202501_RL06v2.0_OBP-ICE6GD_HALFDEGREE.nc, (Loomis et al., 2019a)
162 which contains monthly estimates of time-variable gravity in units of cm equivalent water height,
163 (ii) JPL TELLUS_GRAC-GRFO_MASCON_CRI_GRID_RL06.3_V4;
164 http://grace.jpl.nasa.gov/data/get-data/jpl_global_mascons/, (Wiese et al., 2018), and (iii) the
165 University of Texas Center for Space Research CSR_GRACE_GRACE-
166 FO_RL0603_Mascons_all-corrections.nc, <https://www2.csr.utexas.edu/grace/> (Save et al., 2016).
167 Though we regrid these product to a 1.0 lat / lon grid for commonality with other data, the inherent
168 resolution of GRACE/FO mascon determination is no better than 10^5 km² or roughly 3 degrees
169 latitude / longitude (Wiese et al., 2018).



170 **2.3. Satellite LASER Ranging Data**

171 Prior to GRACE, space based gravimetry was accomplished by satellite laser ranging (SLR) from
172 Earth's surface to mirrored, passive geodetic satellites. After 1993, there were enough laser
173 ranging satellites in orbit to derive mass change time series using the mass concentration (mascon)
174 approach (Rowlands et al. 2005) with sub-continental scale resolution. Herein we use TWS
175 mascon data derived from SLR observations from 5-7 geodetic satellites (Loomis et al. 2019a).
176 The solution time series was adaptively de-seasoned using the Ensemble Empirical Mode
177 Decomposition (Wu and Huang 2009). Mass trends were calibrated by GSFC to match
178 GRACE/FO over a common span to mitigate impacts of parameter correlations, due to internal
179 tests by GSFC that demonstrated that the recovered SLR inter-annual signals are not dependent on
180 the background gravity model, but that the recovered trends are.

181 **2.4. ISIMIP Models**

182 The Inter-sectoral Impact Model Intercomparison Project, ISIMIP, is an international community-
183 driven initiative that provides a consistent framework for multi-model climate-impact simulations
184 across sectors such as water, agriculture, ecosystems, health, and infrastructure and many others
185 (Warszawski et al., 2013; Rosenzweig et al., 2017; Frieler et al., 2024). It does this by establishing
186 protocols for experiments designed to ensure comparability across the multiple sectors and scales.
187 One subset of the most recent modeling efforts is ISIMIP3a and the sector Water_Global. A subset
188 of these model experiments uses historical atmospheric forcing data sets to drive GHMs and LSMs
189 (Gosling et al., 2025). Here we employ TWS data from five models: WaterGAP 2.2e, PCR-
190 GLOBW 2, LPJmL5-7-10-fire, H08 and JULES. Data from three sets of forcing data sets are
191 used. The GSWP3-W5E5 (Cucchi et al., 2020; Lange et al., 2022) adopts ERA5 near-surface
192 meteorology, 1979-2019 over land, with CRU TS4.03 adjustments to two-meter air temperature,
193 T_{2m} , net downward shortwave radiation, SW_d , number of wet days, and GPCP2018 monthly
194 precipitation totals which have been adjusted for bias undercatch. GSWP3
195 (<https://doi.org/10.48364/ISIMIP.982724.1>) is a bias adjusted version of the Twentieth Century
196 Reanalysis v2 (Kim, 2017; Compo et al., 2011) that has been harmonized to reduce biases relative
197 to W5E5 over the 1978-1979 period. The GSWP3-W5E5 forcing has also been used at GSFC to
198 produce a companion experiment with the Global Land Data Assimilation System (GLDAS;
199 Rodell et al., 2004) driving the Noah land surface model. Finally, the ISIMIP3a protocol also



200 makes available a set of experiments to compare the differences between ERA5 and W5E5 forcing:
201 20CRv3-W5E5 and 20CRv3-ERA5. These experiments use the version 3 of the NOAA 20th
202 Century Reanalysis before 1979 (Slivinski et al., 2019), hence the different nomenclature, but they
203 too are bias corrected to either ERA5 or W5E5. Since we confine our analysis to the post 1979
204 period, these bias corrections do not impact our results. We explore differences in these two
205 analysis versions with WaterGAP, LPJ and H08 to quantify these different forcings on TWS
206 evolution. Finally, we note that some of the GSWP3-W5E5 model experiments have additional
207 versions where HWM has been disabled in the models, rendering them “LSM-like”. We use these
208 WaterGAP and LPJ experiment versions. Further details of the ISIMIP3a models used in this study
209 and their formulation are found in Table 1.

210

211



212

ISIMIP Model	Configuration	Hydrology	Human Water Management	Documentation
WaterGAP2.2e	GWHM 0.5 x 0.5 deg res; daily time step 20CRv3_W5E5, 20CRv3_ERA5 used	Canopy, vegetation, snow; single soil layer. Lake, reservoir and river modeling Runoff calibrated against observed streamflow Groundwater recharge, extraction and linear storage / outflow depletion.	Irrigation, domestic use, thermal & manufacturing, livestock Also run with no water management.	Döll et al., 2003 Müller Schmied et al., 2021, 2023. http://watergap.de/
PCR- GLOBWB-2	GWHM 5 arcmin (9 km); daily time step	2 soil, 1 groundwater layers. 4 landcover, soil types, climatologically varying phenology Runoff routing: kinematic wave enabling floodplain inundation Groundwater recharge, capillary rise, riverbed infiltration, linear storage / outflow depletion	Irrigation, domestic, livestock Simple reservoir management	van Beek et al., 2011 Sutanudajaja et al., 2018 http://globalhydrology.nl
LPJmL5-7- 10-fire-Fire	DGVM Experiments used are 20CRv3_W5E5, 20CRv3_ERA5 forcing	5 soil layers: 20, 30, 50, 100, 100 cm Dynamic simulation of growth and productivity (prescribed spatial distribution of crops and pasture) Runoff routing: Continuity equation derived from linear reservoir model	Irrigation determined endogenously. Simple reservoir modeling, industry, domestic uses, prescribed water consumption provided by ISIMIP. Also run as LSM with no water management.	Sitch et al., 2003 Wirth et al., 2024
H08	GWHM 0.5, 0.5 deg res; daily time step 20CRv3_W5E5, 20CRv3_ERA5 used	Single layer climate variable depth. Represents dominant veg for climate zones TRIP-based runoff routing	Abstraction & return flow for river, reservoir, renewable and non-renewable groundwater	Hanasaki et al., 2018. https://h08.nies.go.jp/
JULES-W2	LSM 0.5 x 0.5 deg res; daily time step	4 soil layers, 10, 25, 65, 200 cm Penman-Montieth ET TRIP-based runoff routing Fixed plant types but CO2 fertilization accounting	None	Best et al., 2011 https://jules.jchmr.org/ Oki and Sud, 1998
GLDAS/Noah	Noah LSM 1.0 x 1.0 deg res; 3-hourly time step	4 soil layers, 0 ⁻¹⁰ , 10-40, 40 ⁻¹⁰⁰ , 100-200 cm Seasonally varying green vegetation fraction with constant Leaf area Index	None	Ek et al., 2003 Rodell et al. 2004 https://ldas.gsfc.nasa.gov/gldas

213

214

Table 1: Attributes of models using ISIMIP3a forcings.

215



216

217 **2.5. Statistical / Machine Learning TWS Reconstructions**

218 To supplement our comparison of different modeling strategies we appeal to recently developed
 219 empirical / statistical methods for TWS estimates. Our analysis considers three statistical TWS
 220 reconstructions: (i) Humphrey and Gudmundsson, (2019), (ii) Li et al. (2021) and (iii) Yin et al.
 221 (2023). We refer to these as HG19, Li21 and Yin23, respectively. These statistical strategies vary
 222 in complexity and the number of input variables, but each trains against GRACE/FO TWS mascon
 223 data. HG19 is the simplest, principally relying on precipitation. Details of these approaches and
 224 reference information are provided in Table 2. While none of these reconstructions explicitly
 225 represent HWM, some implicit sensitivity to these factors is present in both Li21 and Yin23.

226

Dataset	Methodology	Input Data Sets	Comments	References
HG19	Linear water store model with spatial autoregressive modeling. Only IA components are modeled. JPL and GSFC mascons	ERA5, GSWP3, MSWEP2.2 precipitation and 2m temperature	Trend, seasonal cycles removed before training; yield is monthly anomalies Trends due to input precip only	Humphrey et al. (2017) Humphrey and Gudmundsson (2019)
Li21	Regionally determined. PCA-like decomposition of predictors. Seasonal, IA, trend components modeled. CSR RL06 GRACE mascons	2m T, NOAA CPC Precip, SST, 17 climate indices	Trained for seasonal cycle and anomalies. Trend pattern is specified from GRACE	Li et al. (2020, 2021)
Yin23	Trained with five different ML models x eight input data combinations JPL, GSFC and CSR mascons	ERA5 hydrometeorological variables + LAI, LULC	Reconstruction extends back to 1940	Yin et al. (2023)

227

228 **Table 2: Significant attributes of three statistical methods for TWS reconstruction.**

229 HG19 produced three different reconstructions using precipitation from either ERA5, the Multi-
 230 Source Weighted-Ensemble Precipitation dataset (MSWEP v2.2; Beck et al. 2017, 2019) or from
 231 the GSWP3 forcing data (Kim, 2017); the GSWP3 dataset has been used to bias correct the 20th
 232 Century Reanalysis (20CR) v2c. HG19 removed trends and seasonality in training against



233 GRACE. Thus, trends in the reconstructed TWS are due solely to trends in input forcing
234 precipitation on which the reconstruction is built. GSWPv3 data extend only through 2014. We
235 exclude the MSWEP-based TWS reconstruction since its precipitation has an unrealistic upward
236 trend compared to GPCC and other precipitation data sets. Using a more complex strategy, Li21
237 first resolve input predictors and GRACE/FO data into 26 river basins. Input predictors are then
238 decomposed using data compression tools (e.g., principal component analysis). GRACE/FO are
239 resolved into seasonal, interannual, residual and trend components and then reconstructed from
240 the predictor data using various ML approaches yielding twelve different estimates. The GRACE
241 trend is enforced in the reconstructions. Selection of the best estimate is done on a regional basis.
242 Yin23 use five different ML approaches but a much larger set of predictors almost exclusively
243 from the ERA5 reanalysis. These predictors are disaggregated into eight different combinations.
244 In sequential fashion, the best performing ML scheme and the best of the eight input configurations
245 in reproducing GRACE/FO TWS is selected. This process is repeated for three GRACE/FO
246 mascon data sets: JPL, CSR and GSFC. Here, we have averaged the three reconstructions.

247 **2.6. Precipitation**

248 The evolution of TWS is strongly related to that of precipitation and its space-time variability (Li
249 et al., 2019; Zhang et al., 2019). In the ISIMIP3a model products examined here, the bias
250 correction of precipitation (e.g. Cucchi et al., 2020) employs monthly means of gridded, gauge-
251 based data from the Global Precipitation Climatology Center (GPCC). In contrast, the ERA5-
252 Land meteorological forcing uses the precipitation generated by the ERA5 atmospheric reanalysis.
253 To assess this influence on the evolution of ERA5-Land TWS we use the GPCC precipitation
254 product GPCC Full 2020 (Schneider et al. 2014), an objectively analyzed gauge-only product
255 gridded to 1.0 degree resolution.

256 Our precipitation analysis is supplemented by two other estimates. The Global Precipitation
257 Climatology Project product GPCPv3.2 (Huffman et al. 2023;
258 <https://doi.org/10.5067/MEASURES/GPCP/DATA304>) merged product blends precipitation
259 estimates from low-orbit satellite microwave data, geosynchronous-orbit satellite infrared data,
260 and sounder-based estimates. Calibration is by GPCC gauge measurements with under / over catch
261 corrections applied. The CRUJRA v2.0 time precipitation analysis (Harris et al. 2021; Kobayashi
262 et al. 2015) is similar in principle to that of W5E5 but instead it adjusts the JRA-55 forcing



263 variables, T_{2m} , q_{2m} , SW_d , P and wet days, to aligned over land to CRU TS (v4.03) data. Here we
264 adopt the resulting precipitation data.

265 Data sets have been re-gridded to 1.0 degree latitude x longitude resolution at monthly time steps
266 and over a domain extending from 60S to 70N. GrADS software was used with box averaging for
267 finer resolutions and bilinear interpolation for coarser resolution datasets. Glaciated grid points are
268 masked, including the Himalayan region, southern South America, coastal portions of the Alaskan
269 / Canadian coast, northern islands of Canada and Greenland. This facilitates comparisons to
270 GRACE/FO by ensuring that we are excluding trends associated with melting ice sheets and
271 glaciers that none of the models simulate. Monthly anomalies are calculated as departures from
272 monthly varying climatologies over the period 2002 to 2019. This period was selected to facilitate
273 comparisons with the GRACE and GRACE-FO products. Given the intrinsic resolution of
274 GRACE/FO of approximately 10^5 km², for comparisons of TWS spatial structure to GRACE
275 products the 1.0 degree model data sets have been smoothed with two applications of a nine-point
276 spatial filter to yield a comparable spatial resolution.

277

278 **3 Results**

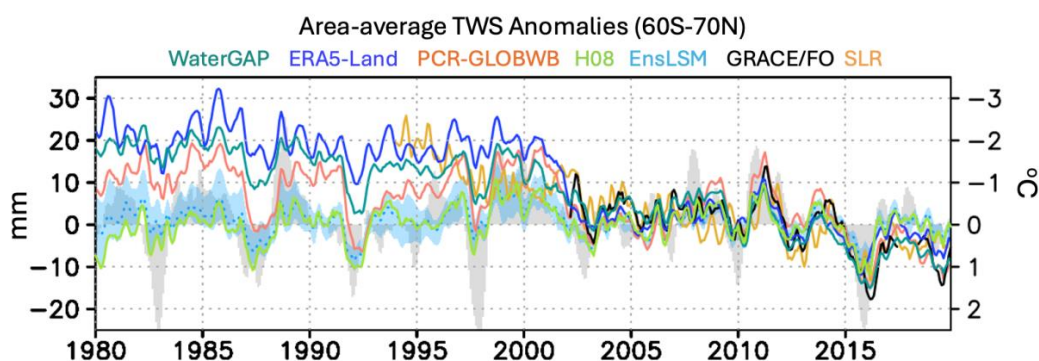
279 **3.1 Global aspects of TWS changes**

280 **3.1.1 Area-average time series**

281 Global mean TWS anomaly time series show striking diversity prior to 2001, yet reasonably
282 consistent agreement thereafter for large interannual signals (Fig. 1). Long-term trends are
283 smallest for the LSMs, which contain no HWM processes (Table 3). This contrasts with the GHMs
284 but should not be surprising given the systematic omission of water use processes in LSMs.
285 However, the relatively close trend agreement between ERA5-Land (-0.80 mm y^{-1}) and WaterGAP
286 (-0.72 mm y^{-1}) over 1980-2019 is surprising given that ERA5-Land contains none of the HWM
287 budget mechanisms contained in WaterGAP (or PCR-GLOBWB). Because the ERA5-Land
288 surface model functions essentially as an LESM, the question then is what drives its large long-
289 term trend? PCR-GLOBWB exhibits an intermediate long-term trend (-0.42 mm y^{-1}), roughly half
290 that of WaterGAP. H08 has a weakly positive TWS trend over the longer period (0.04 mm y^{-1}).



291 Since all of the GHMs are driven by the same meteorological forcing, these differences indicate
 292 uncertainty of TWS changes in the face of GHM model physics differences and their treatment of
 293 HWM processes.



294
 295 **Figure 1: Time series of global area-averaged (60S-70N) Terrestrial Water Storage (TWS)**
 296 **anomalies (mm) from ERA5-Land, GRACE/FO, SLR, three Global Hydrologic Models:**
 297 **WaterGAP, PCR-GLOBWB and H08, an ensemble spread of Land Surface Models: JULES,**
 298 **LPJ, WaterGAP (with HWM disabled), and GLDAS/Noah. The LSM mean is shown as a**
 299 **dotted line. Anomalies are departures from monthly resolved climatologies over the period**
 300 **2002-2019. A 3-month boxcar smoothing has been applied. Nino3.4 SST anomalies, °C, are**
 301 **plotted as gray. The SST scale is inverted to emphasize the tendency for relationship between**
 302 **anomalously warm (cold) SST and depressed (elevated) precipitation over land.**

303
 304 In addition to the trend variations, there are strong coherent interannual signals that relate in large
 305 part to El Niño Southern Oscillation (ENSO) variability; TWS standard deviations (S.D.s) of order
 306 3.5 to 4.5 mm around the trends are typical. PCR-GLOBWB, with three soil layers, has the largest
 307 value of 6.0 mm. Only PCR-GLOBWB approximates the GRACE/FO S.D. value of 4.7 mm during
 308 2002-2019. Sensitivity studies have shown that adding more soil storage capacity notably
 309 increases variability and trends (Döll, personal communication). In the development of ENSO
 310 warm events (1987, 1992, 1997, 2015) significant TWS decreases are observed, reflecting
 311 decreased moisture transport to land and precipitation during warm SST episodes (Trenberth and
 312 Shea, 2005; Miralles et al., 2014; Robertson et al., 2016; Bosilovich et al., 2020). The strong La
 313 Niña SST cooling in 2010 is matched by large TWS increases, behavior consistent with the



314 previously reported dramatic global mean sea level fall of 5 mm in 2011 (Boening et al, 2012).
 315 Relaxation of the strong SST cooling during 2000-2002 that followed the intense 1997/1998 El
 316 Niño is accompanied by strong TWS decreases in ERA5-Land, WaterGAP and PCR-GLOBWB;
 317 it is also present to a lesser extent in the LSMs. However, this 2000-2002 period of significant
 318 change in SSTs and associated TWS decreases also coincides with significant changes in satellite
 319 remote sensing that can bias reanalyses. Precipitation changes over this period in ERA5, which
 320 drives ERA5-Land, have been noted by Wang et al. (2026).

		GHMs			LSMs (No Water Management)				
	GRACE/FO	WaterGAP	PCR-GLOBWB	H08	ERA5-Land	JULES	LPJ NWM	WaterGAP NWM	GLDAS /Noah
Trend									
1980-2019	---	-0.72	-0.42	0.04	-0.80	-0.23	0.36	0.05	-0.05
(2002-2019)	(-0.80)	(-0.91)	(-0.49)	(-0.06)	(-0.40)	(-0.09)	(0.50)	(-0.06)	(-0.01)
S.D.									
1980-2019	---	4.19	5.98	4.24	5.07	4.49	3.34	4.25	3.48
(2002-2019)	(4.68)	(3.86)	(5.76)	(3.78)	(3.39)	(4.03)	(3.57)	(3.76)	(3.29)
Trend Pattern Correlation with GRACE/FO 2002-2019		0.36	0.36	0.25	0.30	0.22	0.27	0.24	0.20
Mean 2002-2019 Anomaly Correlation with GRACE/FO		0.55	0.53	0.47	0.63	0.62	0.55	0.25	0.57

321

322 **Table 3: Various statistics summarizing TWS trends and variability. Trends (mm y⁻¹) and**
 323 **standard deviations (S.D., mm) of TWS time series are made with monthly data without the**
 324 **temporal smoothing in Fig. 1. Calculations are over the 1980-2019 period with values for the**
 325 **2002-2019 period in parentheses. Anomaly correlations are time means of area-averaged**



326 **(60S-70N) monthly correlation maps. For both trend pattern and anomaly correlations, two**
327 **applications of a 9-point spatial filter have been applied to model TWS to approximate the**
328 **intrinsic spatial resolution of GRACE/FO. All anomalies use a monthly resolved climatology**
329 **of 2002-2019.**

330 In contrast to the trend pattern correlations, in which the GHMs are systematically closer to
331 GRACE/FO, the GHM anomaly correlations (just above 0.50) are even lower than for most of the
332 LSMs. Two factors may contribute to these lower correlations. First, the time-integrated effects
333 of water management on trends are likely better modeled than monthly variations of those
334 processes. Second, TWS response to P, ET and RO at 1.0 degree gridpoints is noisy on a monthly
335 time scale, equally affecting GHMs and LSMs. ERA5-Land shows closest agreement with
336 GRACE/FO ($r = 0.63$), the highest of the LSMs, which is confirmation of the consistency of the
337 ERA5 4D-Var assimilation system.

338 **3.1.2 Spatial structure of TWS trends**

339 Though our primary interest is in TWS change over the recent 40-year period, GRACE/FO data
340 extend only from April 2002 onward. For the ISIMIP3a 1980-2019 experiment period this
341 amounts to approximately 17 years. Examining spatial structure of trends over each of these
342 periods (Fig. 2) provides a fuller context of TWS behavior differences resulting from the various
343 modeling strategies. GRACE/FO TWS decreases (Fig. 2a) dominate much of the arid world
344 including the Middle East, Western Russia, but also extending through Europe and North Africa.
345 Focused areas of loss over northern India, northeast China, and the south central U.S. are present
346 where groundwater depletion has been widely documented (Wada et al., 2010; Rodell et al., 2018;
347 Gleeson et al., 2020). TWS declines over southeast Brazil adjacent to gains over the Amazon
348 basin suggest ENSO influence that is unrectified in such a short period; but it may also reflect
349 longer term changing precipitation patterns connected to Atlantic meridional SST gradients (Nobre
350 and Shukla, 1996; Marengo et al., 2017; de Souza Santos et al., 2024) as well as long-term drying
351 from land / ocean warming contrast (Wainwright et al. 2022). Prominent TWS gains over the
352 Sahel and along the Rift Valley southwestward into Angola / Namibia dominate the African
353 continent.

354 Consistent with previous evaluations of modeled TWS (Scanlon et al., 2018; Tiwari et al., 2025),
355 none of the GHMs or LSMs can satisfactorily replicate GRACE trend patterns or magnitudes over

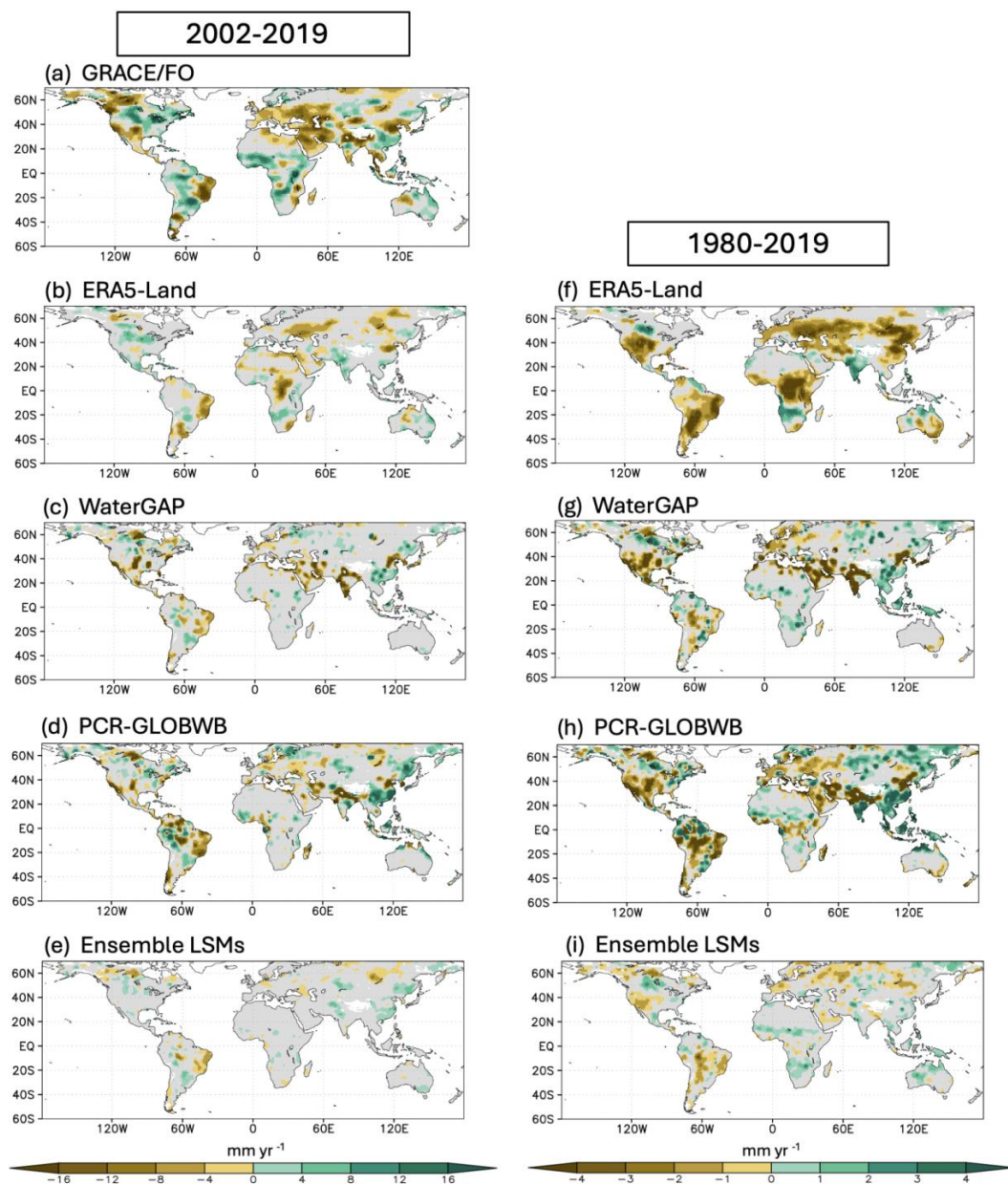


356 the 2002-2019 period; nor does ERA5-Land. WaterGAP and PCR-GLOBWB achieve the largest
357 trend pattern correlation with GRACE (0.36), but this agreement is quite low (Table 2). ERA5-
358 Land is slightly lower (0.30), marginally stronger than the LSMs. Strongest agreement of the two
359 GHMs with GRACE/FO is in regions where groundwater extraction is prominent (Fig. 2 c,d; much
360 of the Middle East, northern India, northeastern China and the U.S. southern plains). Here the
361 GHMs benefit from water use simulations supporting irrigation, industry and human consumption.
362 To the point, the trend pattern for the WaterGAP experiment with no water management
363 (WaterGAP NWM; not shown) looks very close to the LSM mean in Fig. 2e. These effects are not
364 modeled by ERA-Land nor any of the LSMs we examined, thus it's no surprise that these local
365 maxima of TWS depletion are essentially missing in these models. An exception might be for
366 ERA5-Land in TWS-depleted northeast China. This may be due in part to the practice in ERA5-
367 Land of actual evaporation being set to the potential rate in irrigated areas, thus drawing down soil
368 moisture. HWM trends in WaterGAP and PCR-GLOBWB are also prominent in the pre-GRACE
369 period (Fig. 2g, h). These patterns are consistent with the gridded water use patterns assembled
370 by Huang et al. (2018). However, to recover local detail in their analysis these authors made use
371 of patterns of water management derived from previous model integrations of the HWMs
372 examined here to extend country wide water use data.

373 Over central equatorial Africa and the Congo Basin a noticeable downward TWS trend in ERA5-
374 Land contrasts with GRACE/FO and any of the GHMs or LSMs (Figs. 2 b, f). As discussed by
375 many studies (Washington et al., 2012; Nicholson et al., 2014; Maidment et al., 2015; Rodell et
376 al., 2024; Su et al., 2026) this region is poorly sampled by meteorological sensors and rain gauges,
377 making it sensitive to changes in assimilated satellite data on which it must more heavily rely. In
378 terms of the entire 1980-2019 period, this difference between ERA5-Land and the other models
379 becomes more pronounced. Other regions (e.g., northeast China, the east-west band across central
380 Asia, and northern Argentina) also exhibit much stronger TWS depletion in ERA5-Land than
381 either WaterGAP, PCR-GLOBWB, or especially the collection of LSMs. Although some of the
382 large TWS trends may relate to ERA5-Land allowing ET at the potential rate for irrigated crop



383 areas, this cannot explain the drying trends in central Africa, central China or eastern Asia.



384

385

386 **Figure 2: Linear trends of TWS (mm y^{-1}) over the periods 2002-2019 (left) and 1980-2019**

387 **(right). Note the factor of four difference in the color bar scale for the two periods. Ensemble**



388 **LSMs include JULES, LPJ, WaterGAP (with HWM disabled), and GLDAS/Noah. Given the**
389 **intrinsic resolution of GRACE/FO data of approximately 10^5 sq km, about 3.0 degrees in**
390 **middle latitudes, the 1.0 degree resolution model data sets have been smoothed with two**
391 **applications of a nine-point spatial filter to yield a comparable spatial resolution.**

392 **3.2 Regional Time Series**

393 The strong regional structure of the TWS trends among the different models and ERA5-Land
394 motivates examining time series of TWS anomalies in several key regions (Fig. 3). None of the
395 models captures the amplitude of GRACE/FO or SLR variability over central Africa (Fig. 3a) with
396 two large minima in 2004-2005 and 2010-2011; nor can they replicate its upward trend with time.
397 Between the late 1990s and 2002 there was a precipitous decline in ERA5-Land TWS not seen in
398 other models and coinciding with multiple satellite system changes (Selva et al., 2017; Dinz and
399 Toddling, 2020; Hersbach et al., 2020; Wang et al., 2026). A subsequent smaller drop also appears
400 after 2014.

401 Over the Indian subcontinent (Fig. 3b) the initial rise in GRACE/FO TWS and its decline after
402 2014 is well captured only by PCR-GLOBWB. ERA5-Land interannual variability does match
403 that of PCR-GLOBWB but does not capture the elevated TWS in the GHMs prior to 2002.
404 WaterGAP has a much stronger TWS decline but has relatively weak interannual signals.

405

406 The northern Argentina and La Plata Basin region (Fig. 3c) is heavily influenced by ENSO
407 (Ropelewski and Halpert, 1987; Barros et al., 2000; Costa et al., 2024). Coherence of TWS
408 changes at interannual scales among all the model simulations is striking and closely follows
409 GRACE/FO except after 2015. The LSMs agree with the GHMs, suggesting dominance of natural
410 variability. Though ERA5's steep decline in TWS near 2002-2003 is consistent with GRACE/FO
411 and PCR-GLOBWB, it clearly defines a shift between two different epochs in terms of the range
412 of variability of TWS that is not seen in the other models. This TWS decline does not cleanly
413 align with that noted over central Africa in 2000-2002, perhaps due to ENSO influence and other
414 factors such as south Atlantic SST variability (Barros et al., 2000; Kayano et al., 2013).

415

416 The southwestern U.S. (Fig. 3d) has endured recurring droughts over past decades and has
417 depended heavily upon irrigation to sustain agriculture (Elias et al, 2016). A resulting drawdown



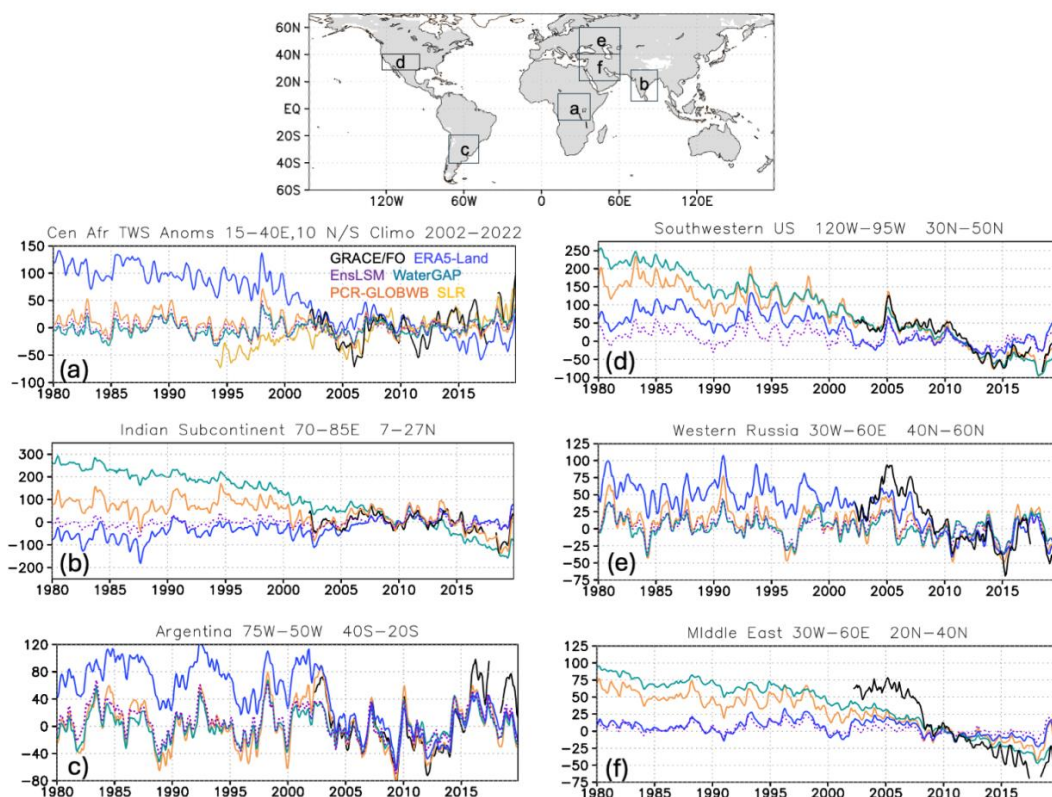
418 in TWS is seen in the GRACE/FO data and is matched closely during that period by WaterGAP
419 and PCR-GLOBWB. Those two models simulate comparable rates over the full 40-year period.
420 ERA5-Land and the LSMs indicate a much more modest decline. Given the dense surface and
421 upper air meteorological observational network over North America, the impact of shifts in
422 satellite observing systems used in ERA5 should be muted in ERA5-land.

423

424 Western Eurasia (Fig. 3e) and areas southward into northern Africa and the Middle East (Fig. 3f)
425 are regions in which all models replicate drawdown of TWS during the GRACE/FO record to
426 varying degrees. Still, none fully capture the amplitude; ERA5-Land and PCR-GLOBWB perform
427 best. There are important differences between the northern and southern halves of this region,
428 which extends from 20S to 60N. Strong interannual variability and an associated downward trend
429 in GRACE TWS characterizes the northern half of the region. A number of studies have examined
430 the recurrence of hydrometeorological drought in this region (Cherenkova et al., 2015; Semenova
431 and Slizhe, 2020 and Semenova and Vicente-Serrano, 2024) and the role of atmospheric warm
432 season blocking episodes, i.e., stationary atmospheric Rossby waves. Of special note are the 2007
433 and 2010 events as evidenced by the Palmer (1965) and Standardized Precipitation and
434 Evapotranspiration Index (SPEI), <https://spei.csic.es/database.html>) drought indices. In the
435 southern half of the region GRACE/FO still shows a strong TWS decline but with a more dramatic
436 decline in 2007 (Fig. 3f). In this region, none of the models adequately capture interannual signals
437 or the associated trend. WaterGAP and PCR-GLOBWB do have long-term downward trends
438 absent in ERA5-Land and the LSMs. We suspect that modeled groundwater depletion, however
439 incomplete and uncertain in these models, may explain the difference. Joodaki et al. (2014) used
440 a combination of GRACE and land surface model estimates of soil, snow, canopy and river water
441 to argue that groundwater depletion dominates during 2003-2014 in this region, centered
442 specifically in Iran. Using a similar strategy, Chao et al. (2017) also reported extraction as the
443 explanation for groundwater depletion within the Tigris-Euphrates Basin over a similar period.



444



445

446 **Figure 3: Regional area-averages of TWS time series anomalies (mm) for ERA5-Land,**
 447 **WaterGAP and PCR-GLOBWB with ensemble LSMs shown as dotted purple lines.**
 448 **GRACE/FO and satellite laser ranging (SLR; global only) based TWS time series are also**
 449 **plotted. Geographic extent of regions is shown in map at top. Anomalies were computed**
 450 **relative to a baseline period of 2002-2019.**

451 Collectively, these different regional views show that relationships between the GHMs,
 452 GRACE/FO and LSMs are not uniform and depend on the hydroclimate of the region (strong
 453 ENSO signals over Argentina; stationary Rossby wave effects over European Russia), the
 454 precipitation gauge density (e.g. Congo basin) and the degree of HWM, especially groundwater
 455 extraction (India and parts of the Middle East). There are, however, systematic differences in the
 456 TWS behavior of the GHMs and ERA5-Land pre- and post-2000/2002. The Congo Basin and
 457 northern Argentina are the most prominent examples. There is evidence, too, over the

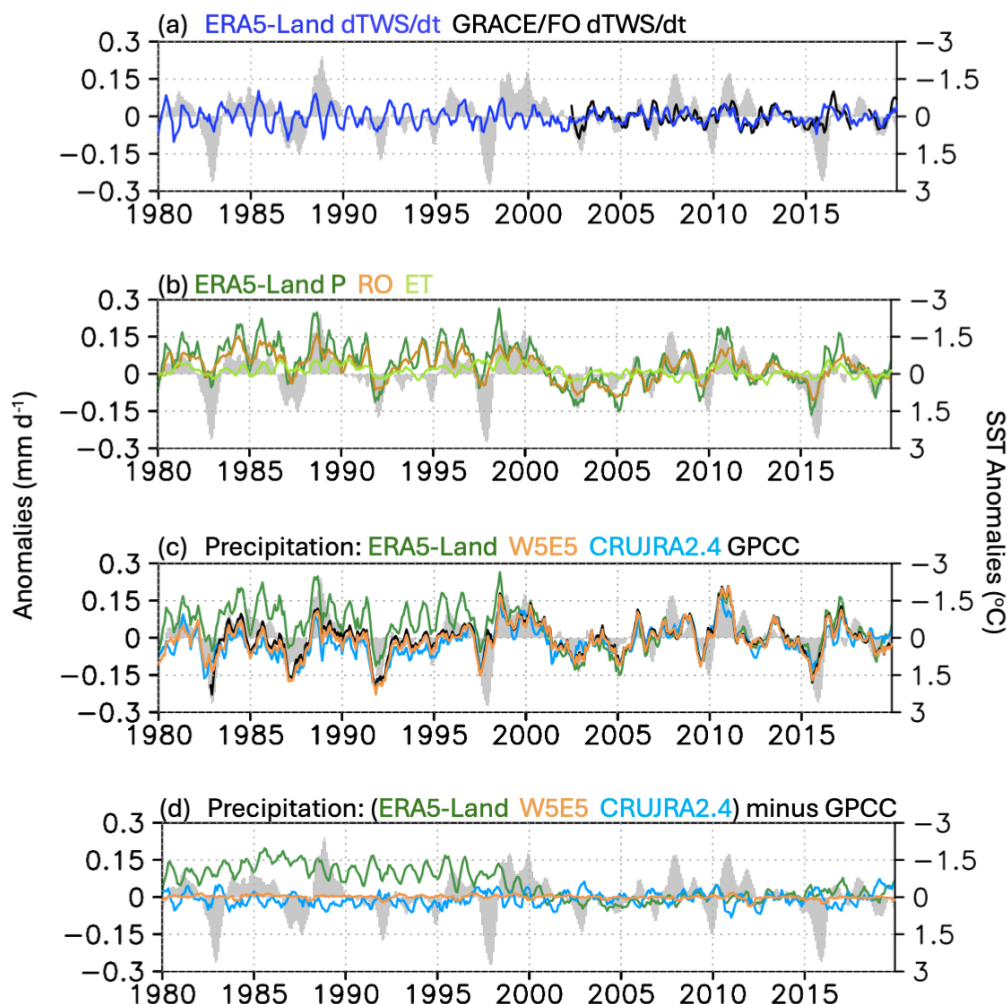


458 southwestern U.S., where ERA5-Land and the ensemble LSM TWS signals diverge during the
459 2000-2002 period.

460 **3.3 Precipitation Differences**

461 The systematic differences between ERA5-Land, GRACE/FO, and model TWS behavior (Figs. 2,
462 3) leads us to investigate the differences in atmospheric forcing, especially precipitation, compared
463 to observation based estimates. Time series of global land area-average ERA5-Land and
464 GRACE/FO anomalies in TWS tendency ($dTWS/dt$), and ERA5-Land P, ET, and RO are shown
465 in Figs. (4a,b). P variations have the largest amplitude followed by those of RO. Phasing of these
466 two quantities is anticorrelated with variations in Nino3.4 SST anomalies, suggesting that SST
467 variations control moisture transport between land and ocean (Trenberth and Shea, 2005;
468 Ropelewski and Halpert, 1987; Robertson et al., 2020). Notably, ERA5-Land P and RO anomalies
469 exhibit significant declines during the 2000-2002 period. These declines do coincide with a
470 transition of cold to warm SSTs in Nino3.4. What is apparent though is that this juncture marks a
471 change in ERA5-Land P and RO behavior before and after this period; both variables are
472 systematically elevated before 2000 compared to the period 2002-2019 (which was used as a
473 baseline for computing anomalies). An important aspect, too, is a strong annual signal in P, RO
474 and $dTWS/dt$ anomalies that emerges before this time. This suggests that the climatology of
475 ERA5-Land, at least its hydrological quantities, differs between these two epochs as is noted in
476 Wang et al. (2026).

477 A defining characteristic of satellite remote sensing from 1980 to the present is the jump in the
478 number of observations, their spectral diversity, spatial resolution and accuracy, especially during
479 the middle of this period (Gelaro et al., 2017; Hersbach et al., 2020). We suspect that the transition
480 from TOVS to ATOVS sounders during 1998-2002 as well as the subsequent availability of AIRS
481 profiles in 2002 enabled improved assimilated temperature and moisture data that systematically
482 changed the ERA5 hydrology (Fig. 4a,b). Just as important is improved temporal coverage of
483 passive microwave imagers in the late 1990s relative to measurements that began in late 1987. In
484 effect, more frequent and better data allowed a stronger, more accurate correction, via data
485 assimilation, of physics biases in the ERA5 model. ERA5-Land inherits the shifting biases in near
486 surface meteorology, precipitation and radiation. A direct goal of W5E5 adjustments was to
487 mitigate these biases where possible using in situ observations (Cucchi et al., 2020).

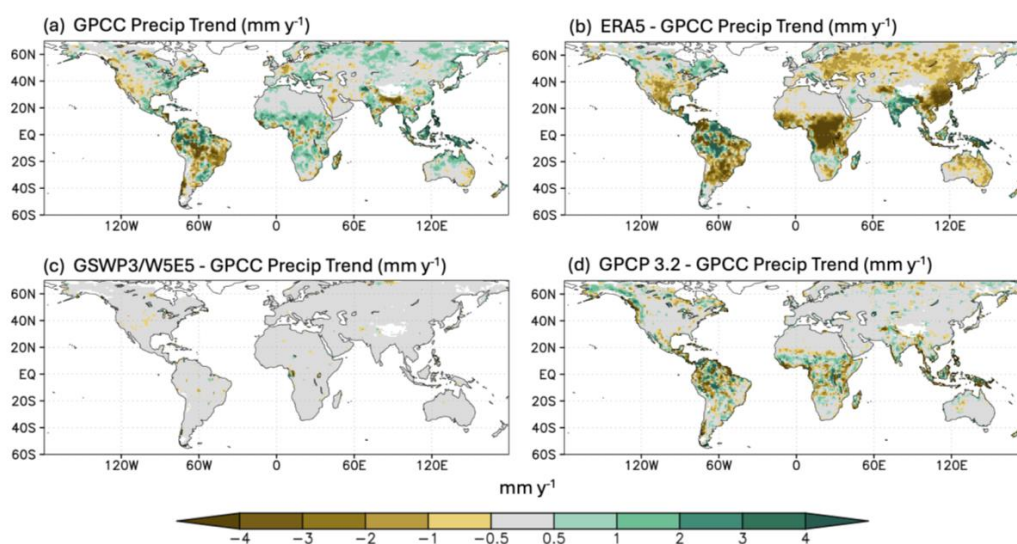


488

489 **Figure 4: Time series of various global area-average (60S-70N) quantities, units mm d^{-1} :** (a)
 490 **ERA5 and GRACE/FO TWS tendencies, (b) ERA5-Land P, RO and ET, (c) Precipitation**
 491 **for ERA5-Land, W5E5, CRUJRA2.4 and GPCC gauge amounts, (d) Same as in (c) but as**
 492 **differences from GPCC. Nino3.4 SST anomalies, °C, are plotted as gray. The SST scale is**
 493 **inverted to emphasize the tendency for relationship between anomalously warm (cold) SST**
 494 **and depressed (elevated) precipitation over land. A 5-month smoother has been applied to**
 495 **the data. Anomalies were computed relative to a baseline period of 2002-2019.**



496 Evidence of these turn-of-century changes is seen in time series of global mean (60S / 70N Land)
 497 monthly precipitation from ERA5 (which are used as inputs to ERA5-Land), the GEWEX Soil
 498 Wetness Project-WATCH Forcing Data-ERA5 (GSWP3-W5E5), [[https://doi.org/10.5194/essd-12-](https://doi.org/10.5194/essd-12-2097-2020)
 499 [2097-2020](https://doi.org/10.5194/essd-12-2097-2020)], and CRUJRA 2.2 (<https://www.nature.com/articles/s41597-020-0453-3>) (Fig. 4c).
 500 ERA5 P values that are elevated relative to the best observationally constrained, bias-corrected
 501 estimates are prominent before the late 1990s. Figure 4d shows this clearly, plotting the
 502 differences between GPCP gauge precipitation and ERA5, W5E5 and CRUJRA2.4. Note that the
 503 latter two precipitation data sets are heavily anchored to GPCP.



504

505 **Figure 5: GPCP precipitation trend (a), mm yr⁻¹, and differences from (b)ERA5, (c) W5E5,**
 506 **and (d) GPCP v3.2. Trends are computed over the 1980-2019 period.**

507 The spatial structure of these differences from GPCP precipitation, especially the resulting trend
 508 pattern, strongly resembles the ERA5-Land TWS trend itself (Fig. 5b vs Fig. 2f). Stronger ERA5
 509 precipitation declines are prominent over central Africa and southeast China, but they are also seen
 510 over parts of Asia, the western U.S. and much of South America. Excessive precipitation gains
 511 over India also correspond to excessive TWS increases. Weaker correspondence is present across
 512 much of Asia and over N. America. The GSWP3-W5E5 precipitation forcing for ISIMIP model
 513 experiments differs negligibly from GPCP by construction. The resulting GPCPv3.2 - GPCP
 514 trend difference pattern has more structure than W5E5 - GPCP but much less than in the case of

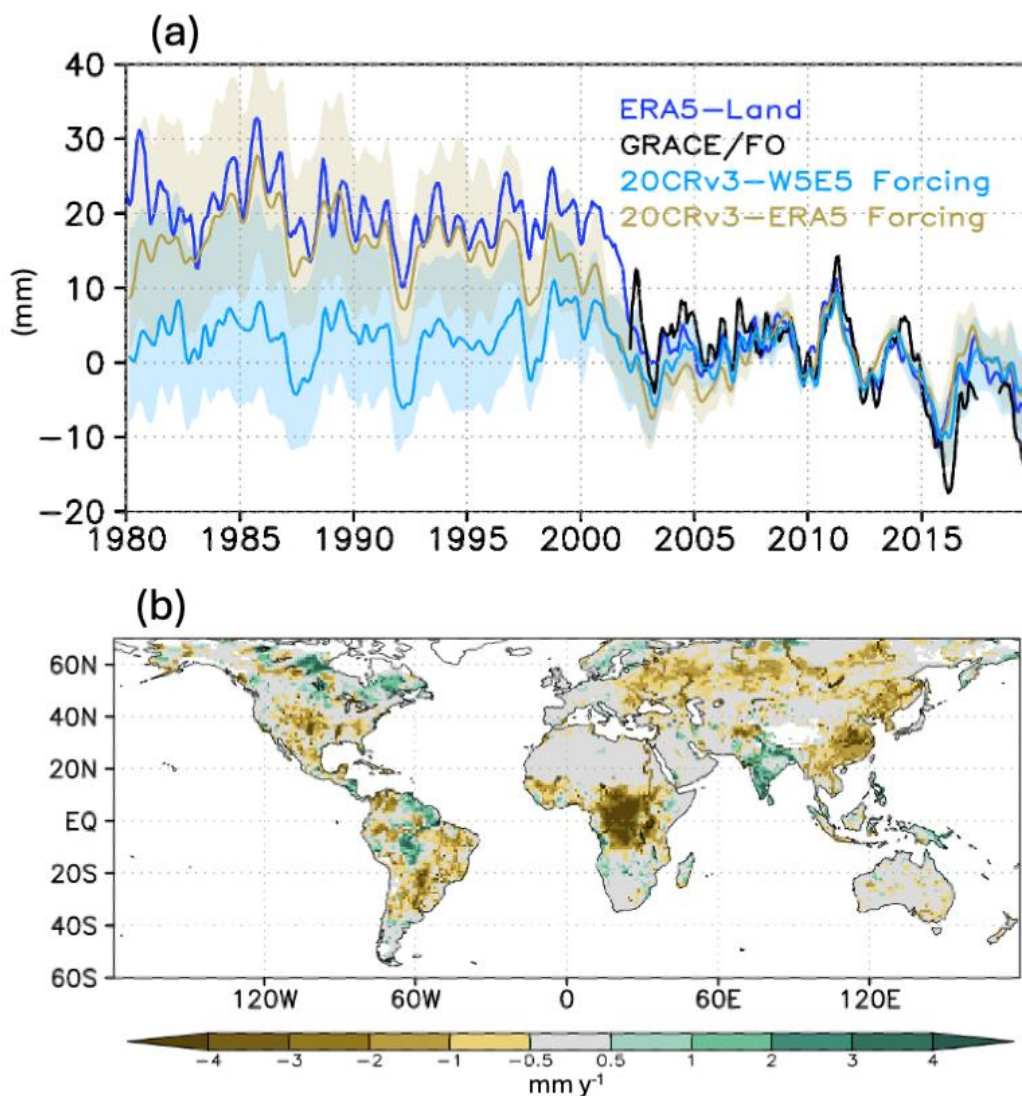


515 ERA5-Land. CRUJRA2.2 differences from GPCC (not shown) are similarly small. These
516 comparisons indicate that the systematic differences between ERA5-Land and other model
517 simulated TWS declines are linked to the precipitation forcing sources.

518 **3.4 ERA5 vs W5E5 Hydrological Forcing**

519 The impact on TWS of the large, seemingly unrealistic decline in ERA5-Land precipitation
520 around 2001-2003 is confirmed by comparing the means of three different ISIMIP3a models (Fig.
521 6a). Shading denotes the three-model spread of TWS around the means. While there are differences
522 among the models, the systematic increase in TWS decline resulting from ERA5 compared with
523 W5E5 forcing is apparent. WaterGAP, LPJ and H08 have anomaly differences between the pre-
524 and post-2000 periods of approximately 10 mm. These results are consistent with the changes in
525 precipitation forcing in ERA5 relative to the ISIMIP3a precipitation, the latter of which employs
526 GPCC gauges to bias-corrected ERA5 precipitation (Fig. 4c,d; Fig 5b).

527 The regional expression of the global mean time series is seen in an ensemble of the ERA5 minus
528 ISIMIP forced TWS trends (Fig. 6b). The ensemble mean difference map of TWS trends shows
529 prominent discrepancies over central Africa and eastern China with weaker systematic variations
530 over Asia and the Americas. These patterns align with the precipitation differences between the
531 two forcing data sets (Fig. 5b) as well as with the 1980-2019 ERA5-Land TWS trends in Fig. 2f.



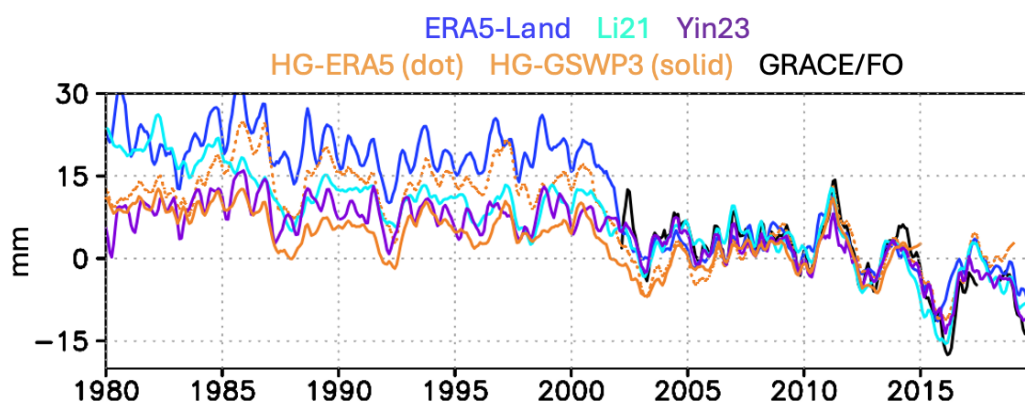
532

533 **Figure 6: (a) TWS time series for two ensembles of three GHMs (WaterGAP, H08 and LPJ)**
534 **but each ensemble under different forcing. The light blue line indicates forcing by the W5E5**
535 **data during 1979-2019 which is based on 20CRv3-W5E5, the observational bias correction**
536 **of ERA5 meteorology. The tan line is for models run with 20CRv3-ERA5 meteorological**
537 **forcing. Shading indicates the spread of the three GHMs. A 5-month smoother has been**
538 **applied to the data. See text for additional discussion. (b) 1980-2019 TWS trend difference**
539 **(mm yr⁻¹) for the ensemble GHMs, ERA5 minus W5E5 forcing.**



540 **3.5. Statistical / Machine Learning TWS Reconstructions**

541 Statistical reconstructions take advantage of covariant relationships between
 542 hydrometeorological state and flux variables so as to replicate GRACE/FO TWS and therefore
 543 serve as a basis for reconstructing TWS in the pre-GRACE/FO era. Global mean TWS time series
 544 from this approach are shown in Fig. 7. Trends, S.Ds. of anomalies, and anomaly correlations
 545 with respect to the detrended time series are given in Table 4.



546

547 **Figure 7: Time series of globally averaged TWS estimates from various statistical**
 548 **reconstructions. ERA5-Land, SLR and GRACE/FO are shown for reference.**

549 TWS in each of the four reconstructions trend downward over the 1980-2019 period and with
 550 magnitudes less than that of ERA5-Land. By design Li21 assumes the GRACE/FO trend pattern
 551 which, as noted by the authors, is likely inaccurate for longer periods of time where climate is non-
 552 stationary and HWM also changes. Yin23 is the only reconstruction that specifically tries to match
 553 the full GRACE/FO variability including the trend, but its input data are almost exclusively from
 554 ERA5. HG19 provides two contrasting TWS realizations, each constrained by precipitation input.
 555 When developed using ERA5 precipitation (HG-ERA5), the 2002-2018 trend (-0.81 mm y^{-1})
 556 nearly replicates GRACE/FO. HG19 using GSWP3 precipitation (HG-GSWP3) is actually
 557 positive (0.29 mm y^{-1}) over the GRACE/FO period, but this reflects the fact that GSWP3 ends in
 558 2014, hence HG19-GSWP3 lacks the strong downturn in TWS after 2014 seen in the models and
 559 other reconstructions. The trend changes to -0.30 mm y^{-1} over the longer period. None of the
 560 reconstructions have trends as large as ERA5-Land over the 1980-2019 period. The HG19
 561 reconstructions also show the weakest interannual signals over both periods. Though Yin23 has



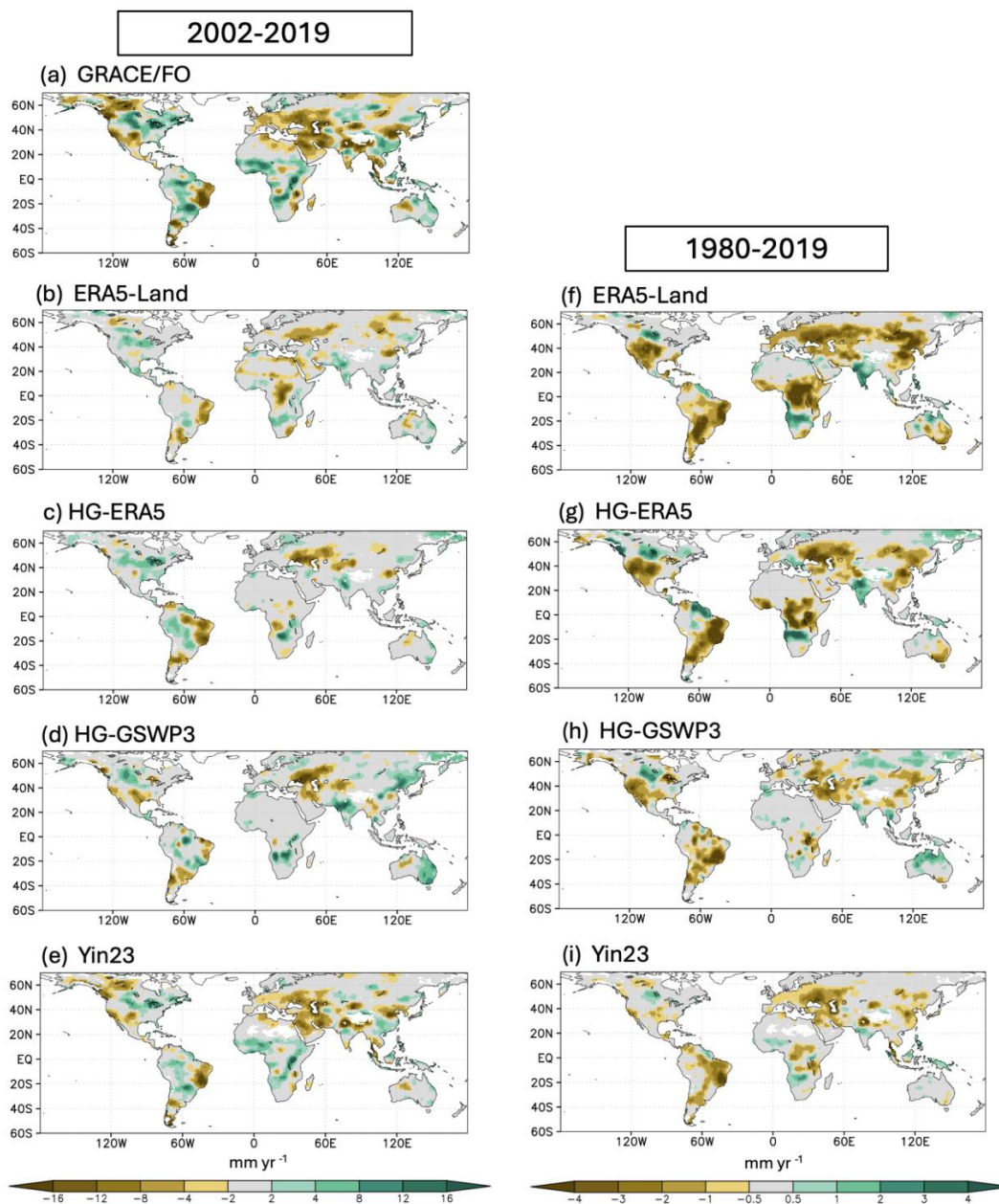
562 arguably the most complex methodology and the largest number of input predictors, it also exhibits
 563 weak interannual changes compared to GRACE/FO. The reconstructions are consistently better
 564 correlated with GRACE/FO than are the models. It's important to keep in mind that this is by
 565 construction. As Li21 notes, enforcing a strong fit to GRACE/FO trend data prior to 2002 carries
 566 significant uncertainty and a stationary trend pattern is unlikely.
 567

	HG19 GSWP3*	HG19 ERA5	Li21	Yin23	ERA5- Land	GRACE/FO
Global Mean Trend 1980-2019 (2002-2019)	-0.30 (0.29)*	-0.53 (-0.81)	-0.63 (-0.67)	-0.40 (-0.63)	-0.80 (-0.40)	--- (-0.80)
S.D. 1980-2019 (2002-2019)	3.18 (2.86)*	5.27 (3.39)	3.89 (4.50)	3.50 (3.22)	5.07 (3.39)	--- (4.68)
Trend Pattern Correlation with GRACE/FO 2002-2019	0.26*	0.36	0.92	0.95	0.30	
Mean 2002 ⁻¹ 019 Anomaly Correlation with GRACE/FO	0.68*	0.78	0.80	0.94	0.63	

568 * GSWPv3 only extends through 2014, thus limiting the training to GRACE during 2002-2014 and failing to sample the lower
 569 TWS values and strong variability present 2015-2019.

570 **Table 4: Same as in Table 2 except for statistically-based TWS reconstructions. Trends are**
 571 **mm y⁻¹ and standard deviations, S.D., are mm. ERA5-Land and GRACE/FO values are also**
 572 **reproduced from Table 2.**

573 Figure 8 maps reconstructed TWS trends over 2002-2019, with ERA5-Land and GRACE/FO
 574 included for comparison. Li21 trends are not shown since by construction they are essentially
 575 identical to those of GRACE/FO (Fig 8a). Yin23 successfully matches the full GRACE/FO
 576 variability and, thus, also matches its pattern closely (0.95; Table 4). The slightly lower correlation
 577 for Li21 (0.92) may be due to their training with a single data set, CSR GRACE TWS, while our
 578 GRACE data is the average of GSFC, JPL and CSR versions, the same combination used by Yin23.
 579 To the extent that HWM explains trend structure, it is implicitly



580

581 **Figure 8: Linear trends of TWS (mm yr^{-1}) over the periods 2002-2019 (left) and 1980-2019**
582 **(right) for various statistical reconstructions. ERA5-Land and GRACE/FO are shown for**
583 **reference. Note the factor of four difference in the color bar scale for the two periods. Given**
584 **the intrinsic resolution of GRACE/FO data of approximately 10^5 sq km, about 3.0 degrees**



585 **in middle latitudes, the 1.0 degree resolution model data sets have been smoothed with two**
586 **applications of a nine-point spatial filter to yield a comparable spatial resolution.**

587 captured in these two reconstructions (e.g., strong TWS declines over northwest India; Fig. 8e,i).
588 In contrast, trend structure in the two HG estimates represent precipitation effects alone. Though
589 many large-scale trend features are similar for these reconstructions (e.g., TWS declines over
590 western Russia, the Middle East, eastern Brazil, northeastern China), significant differences from
591 GRACE/FO regional details are present. Not surprisingly, HG-ERA5 indicates a generally
592 negative TWS trend over central Africa while HG-GSWP3 captures at least some of the largely
593 positive trends detected by GRACE/FO.

594 Over the 1980-2019 period HG-ERA5 replicates much of the large amplitude trend structure
595 seen in ERA5-Land, attesting to the primacy of precipitation forcing. HG-GSWP3 and Yin23
596 agree in the much weaker decreases over central Africa, Argentina and northeastern China
597 compared to ERA5. However, only Yin23 weakens the TWS losses over southwest North
598 America.

599

600 **4 Discussion and Conclusions**

601 Our analysis has considered a range of physical modeling and statistical approaches to
602 reconstructing TWS in the pre-GRACE/FO era: GHMs, LSMs, the ERA5-Land reanalysis and
603 statistical / ML methods. The bulk of these estimates support a continued global drawdown of
604 TWS since the 1980s. However, the range of resulting trend estimates from near zero to -0.9 mm
605 yr^{-1} (Tables 3, 4) and their differences in spatial structure (Figs. 5,8) are substantial. These results
606 highlight the challenges inherent in quantifying TWS variability before routine GRACE/FO
607 gravimetric measurements became available. To summarize our findings:

608 1. ERA5 is affected by a stepwise change in the observing system producing an unrealistic decline
609 in precipitation from before to after 2000-2002, which was implied by earlier work (Hersbach et
610 al. 2020; Allan 2023; Wang et al. 2026). This is evidenced by comparison of ERA5 and the
611 GSWP3-W5E5 precipitation and confirmed by ISIMIP3a GHM models forced by ERA5 versus
612 ISIMIP3a W5E5 meteorology; for three ISIMIP3a models ERA5 forcing leads to global mean
613 TWS being at least 15 mm higher prior to 2000. These artifacts are small and largely unimportant
614 for many applications of ERA5-Land which focus on short time scales (i.e., days to months) but



615 they are of comparable size to many climate variability and change signals. Numerous
616 investigations have demonstrated that ERA5 and ERA5-Land are significant improvements over
617 previous reanalysis efforts (Muños-Sabater et al., 2021; Wang et al., 2022). ERA5-Land supports
618 an ever wider variety of investigations of land surface hydrology (e.g., Liu et al., 2020; Clelland
619 et al., 2024; Wang et al., 2026). All reanalyses contend with physics biases and assimilate
620 observations whose quality and coverage varies with time. Our results here clarify aspects of TWS
621 behavior in ERA5-Land of which users studying multi-decadal variability must be aware.

622 2. Our analysis also shows that GHMs, even when driven with state of the art, bias corrected
623 meteorology can yield global TWS trends and associated regional structures that differ
624 systematically from those observed by GRACE/FO. We reaffirm the results of Scanlon et al.
625 (2018) and Tiwari et al. (2025) that GHMs have difficulty capturing the amplitudes of trends seen
626 by GRACE/FO. The spread of global mean trends in just three GHMs, from -0.06 to -0.91 during
627 the GRACE/FO period and 0.04 to -0.80 mm y⁻¹ over 1980 to 2019, attest to the remaining
628 challenges. The degree to which this is due to internal model physics and parameters (e.g., depth
629 of the saturated zone and soil storage capacity, the still rudimentary treatment of groundwater,
630 landcover / land use changes) or the (lack of) treatment of HWM remains unknown.

631 3. The incorporation of HWM does make crucial contributions in many regions (e.g., northern
632 India, northeast China and southern Great Plains). Without accounting for HWM, WaterGAP
633 global TWS trends over 2002-2019 change from -0.40 mm y⁻¹, roughly half the GRACE/FO value,
634 to -0.06 mm y⁻¹. We have used only a subset of the full range of ISIMIP3a models, and examining
635 details of their relevant process representations would be a valuable next step. Telteu et al. (2021)
636 and Muller-Schmied et al. (2025) offer a needed framework for consistency in defining model
637 physics and comparing GHM output that allows experiments to isolate model shortcomings.

638 4. Finally, we considered a third methodology of TWS estimation that involves training statistical
639 models to replicate TWS variability seen in the GRACE/FO record and then projecting these
640 statistical reconstructions back before 2002. To varying degrees these reconstructions are able to
641 capture the global imprint of interannual variability associated with ENSO. In terms of TWS
642 trends, the input data sets have some issues. Li21 only models seasonal and interannual TWS
643 signals and just embeds the linear trend taken from GRACE/FO. The fidelity of this assumption
644 encompassing the entire 1980-2019 period is questionable. Yin23 use by far the largest set of



645 predictors but virtually all are taken from the ERA5 reanalysis without any recourse to bias
646 correction. Nevertheless, the prominent decline in ERA5-Land TWS during the 2000-2002 period
647 is damped in Yin23. Since the precipitation input is the same in these two products, it is not clear
648 what factors, training algorithm strategy or data input, produce this behavior. The HG-GSWP3
649 reconstruction does not take advantage of the full GRACE/FO record. Yet, it does indicate that
650 precipitation forcing by itself produces a downward trend over the 1980-2019 period. Common
651 to all these methods, though, is that no direct accounting of HWM is present. While to some
652 degree these effects are present implicitly in Li21 and Yin23, this is a distinct limitation of all
653 present statistical TWS reconstructions.

654 Taken as a whole, all three methodologies, the ERA5-Land reanalysis, GHMs and statistical
655 approaches, strongly support continued drawdown of TWS in many regions over the full 40-year
656 period starting in 1980: the dry lands of western Russia, the Middle East, northern India,
657 southeastern Brazil, and parts of the southwestern U.S. Of these methods we argue that the ERA5-
658 Land regional amplitudes and global trend are unrealistically large, likely due to non-physical
659 ERA5 precipitation changes, although we cannot estimate the amount accurately. Furthermore,
660 since ERA5-Land does not account directly for HWM, these effects might restore a large trend
661 were they included in an experiment with bias-corrected forcing. WaterGAP and PCR-GLOBWB
662 each produce TWS declines, most likely determined by HWM effects. It is noteworthy that the
663 HG-GSWP3 and Yin23 statistical / machine learning reconstructions also produced downward
664 trends, -0.30 and -0.40 mm y^{-1} , respectively; the former is from precipitation forcing only while
665 the latter implicitly includes at least some HWM effect. For all these estimates it should be
666 emphasized that interannual variability and longer term decadal processes likely influence trends
667 on this scale substantially. Ultimately a process understanding behind any trend estimates needed
668 to make them useful for planning.

669 Some recommendations for the future as a result of this study include:

670 (i) Continued refinement and improvement of bias correction for model forcing. This study has
671 illustrated how diversity of reconstructed global mean TWS trends and their constituent regional
672 contributions is sensitive to forcing data, most notably precipitation. The ISIMIP3a experiments
673 contrasting ERA5 versus the bias corrected W5E5 (Fig. 6) clearly point to this issue. The
674 hydroclimate community has expended substantial effort developing methods to minimize bias in



675 forcing data sets (Sheffield and Wood, 2007; Wheedon et al., 2011, 2014; Cucchi et al., 2020).
676 The rapid maturation of passive microwave imaging, the transition from TOVS to ATOVS
677 sounding and increased aircraft reports all challenge bias-correction efforts. The reliance of
678 assimilation systems on temporally inconsistent observations to correct model physics biases is a
679 perennial problem.

680 (ii) An especially important component of bias correction is precipitation. All gridded forcing
681 data for models, whether model or satellite sensor based, are ultimately calibrated based on in situ
682 gauge records, which are widely known to have issues with heterogeneity of geographic coverage,
683 inconsistent and ephemeral temporal coverage and access restrictions stemming from geopolitical
684 issues (Famiglietti et al., 2015). Improved access to data records has been made through “data
685 archaeology” (e.g. Nicholson et al., 2014; Thorne et al., 2017; Chimani et al., 2022). Efforts like
686 these to bolster poorly sampled regions and countries need more emphasis.

687 (iii) Improved fidelity of HWM simulations in GHMs. Despite efforts to accommodate
688 groundwater storage and its governing processes in GHMs, the treatment remains simplistic and
689 suffers from sparse measurement density needed to sample different hydroclimate regimes. Other
690 HWM aspects such as reservoir and river flow management, changes in local lakes with drought
691 and inundation with drought are all needing improvement. But this attention to HWM must be
692 supported by improved GHM physics such as biophysical processes, soil properties and layer
693 structure. The methodology for standardizing model process definitions for archival (Telteu et al.,
694 2021) is a contribution that will greatly facilitate model intercomparison and improvement.
695 Extending and improving regional details of water use and groundwater extraction (Huang et al.,
696 2018) for validating models is crucial.

697 (iv) While differing in concept from physical modeling, statistical ML, AI and deep learning
698 methods will likely advance these efforts. As the GRACE/FO record lengthens and samples more
699 modes of TWS variability these methods could offer insight on how various hydrometeorological
700 inputs contribute to TWS variability, contingent of course on adequate bias treatment of training
701 data.

702 In summary, our findings indicate that previously documented TWS decline since 2002 extend
703 back over the past four decades and are explained by coincident decline in regional precipitation
704 combined with a growing influence of HWM, though the magnitude of this global and regional



705 drying is poorly quantified. We urge caution in interpreting reanalyses, model produced data sets,
706 or any reconstructed estimates that have not used bias corrected forcing data. The present study is
707 just a snapshot of current efforts to extend understanding of TWS variability to years before space-
708 based gravimetry began to make definitive measurements of water stores and their evolution.
709 Though all reconstruction techniques are just estimates, prospects for narrowing their uncertainties
710 and improving the historical understanding of this component of the global water cycle are
711 encouraging and important to water resource and ecosystem management.

712

713 **Appendix A List of Acronyms**

714

715	Acronym	Full Form
716	AIRS	Atmospheric Infrared Sounder
717	ATOVS	Advanced Tiros Operational Vertical Sounder
718	CRUJRA	Climatic Research Unit Japanese Reanalysis
719	CSR	Center for Space Research
720	DVM	Dynamic Vegetation Model
721	ENSO	El Niño–Southern Oscillation
722	ERA5	Fifth generation ECMWF atmospheric reanalysis
723	ERA5-Land	Land component of ERA5 reanalysis
724	GHM	Global Hydrology and Water Resource Model
725	GLDAS	Global Land Data Assimilation System
726	GPCC	Global Precipitation Climatology Centre
727	GPCP	Global Precipitation Climatology Project
728	GRACE	Gravity Recovery and Climate Experiment
729	GRACE-FO	Gravity Recovery and Climate Experiment – Follow-On
730	GSFC	Goddard Space Flight Center
731	HCTESSEL	Carbon Hydrology-Tiled Scheme for Surface Exchanges over Land
732	HWM	Human Water Management
733	IA	Interannual
734	ISIMIP	Inter-sectoral Impact Model Intercomparison Project
735	ISIMIP3a	Third round of ISIMIP experiments (phase a)



736	JPL	Jet Propulsion Laboratory
737	LSM	Land Surface Model
738	LESM	Land Earth System Model
739	LULC	Land Use / Land Cover
740	ML	Machine Learning
741	SLR	Satellite Laser Ranging
742	SPEI	Standardized Precipitation and Evapotranspiration Index
743	SST	Sea Surface Temperature
744	TOVS	Tiros Operational Vertical Sounder
745	TWS	Terrestrial Water Storage
746	UEA	University of East Anglia
747	WATCH	Water and Global Change initiative
748	W5E5	WATCH de-biasing methodology applied using ERA5 data over land and ERA5
749		data over ocean

750

751 **Code and Data Availability**

752 ISIMIP3a model experiment output,

753 https://data.isimip.org/search/tree/ISIMIP3a/OutputData/water_global/

754 PCR-GLOBWB 2 model experiment output, contact edwin.sutanudaja@uu.nl

755 <http://globalhydrology.nl>

756 ERA5_Land Reanalysis

757 <https://cds.climate.copernicus.eu/datasets/reanalysis-era5-land?tab=overview>

758 Precipitation:

759 GPCP Full 2020: <https://psl.noaa.gov/data/gridded/data.gpcp.html>,

760 GPCPv3.2, <https://doi.org/10.5067/MEASURES/GPCP/DATA304>;

761 CRUJRA, <https://catalogue.ceda.ac.uk/uuid/10d2c73e5a7d46f4ada08b0a26302ef7>

762 GRACE Mascon TWS:

763 GSFC, <https://earth.gsfc.nasa.gov/geo/data/grace-mascons>

764 JPL http://grace.jpl.nasa.gov/data/get-data/jpl_global_mascons/

765 CSR <https://www2.csr.utexas.edu/grace/>

766 SLR Mascon TWS: <https://earth.gsfc.nasa.gov/geo>, contact bryant.d.loomis@nasa.gov



767

768 GRACE-Like TWS Reconstructions

769 Humphrey and Gudmundsson (2019): <https://doi.org/10.6084/m9.figshare.7670849>

770 Li et al. (2021): <https://datadryad.org/dataset/doi:10.5061/dryad.z612jm6bt>

771 Yin et al.(2023): <https://doi.org/10.5281/zenodo.10040927>

772 GLDAS-Noah Experiment with W5E5 Forcing: <https://ldas.gsfc.nasa.gov/gldas>, contact
773 hiroko.beaudoing@nasa.gov

774

775 **Author Contributions**

776 FRR conceptualized the study in consultation with all other authors, produced and executed the
777 analysis code, and produced the initial draft. MGB helped develop Grads analysis and graphics
778 code. MR led analysis of GRACE diagnostics. RPA led in critical structuring of paper, JM-S
779 analyzed and critiqued ERA5-Land diagnostics, BL developed the SLR TWS retrievals. HB
780 produced the Noah-GLDAS experiment data, JBR assisted in discussion of ML techniques. All
781 authors contributed substantially to writing the manuscript, providing critical feedback and
782 approving the final draft.

783

784 **Competing Interests**

785 The contact author has declared that none of the authors has any competing interests.

786

787 **Acknowledgements**

788 The authors express their thanks to the modeling teams who contributed to the ISIMIP 3a Global
789 Water initiative, especially Hannes Müller Schmied, Goethe-University Frankfurt, Frankfurt,
790 Germany; Edwin Sutanudjaja, Department of Physical Geography, Utrecht University; Naota
791 Hanasaki, National Institute for Environmental Studies (Japan); Sebastian Ostberg, Potsdam
792 Institute for Climate Impact Research; Emmanouil Grillakis, Technical University of Crete. The
793 authors also acknowledge the authors and teams who have developed and made available
794 statistically-based TWS estimates: Vincent Humphrey, Institute for Atmospheric and Climate
795 Science, ETH Zurich, Zurich, Switzerland; Fupeng Li, College of Marine Science and
796 Technology, China University of Geosciences, Wuhan, China; Jiabo Yin, State Key Laboratory
797 of Water Resources Engineering and Management, Wuhan University, Wuhan, Hubei, PR China.



798

799 **Financial Support**

800 FRR acknowledges the NASA / MSFC Emeritus Program for access to computational resources.

801 FRR, MGB, MR, HB and JBR also acknowledge support from the NASA Energy and Water Cycle
802 Study, Dr. Craig Ferguson, Program Manager.

803

804 **References**

805 Adams, K. H., Reager, J. T., Rosen, P., Wiese, D. N., Farr, T. G., Rao, S., and et al.: Remote
806 Sensing of Groundwater: Current Capabilities and Future Directions, *Water Resources*
807 *Research*, 58, 27, <https://doi.org/10.1029/2022wr032219>, 2022.

808 Allan, R. P.: Amplified seasonal range in precipitation minus evaporation, *Environmental*
809 *Research Letters*, <https://doi.org/10.1088/1748-9326/acea36>, 2023.

810 Barros, V., Gonzalez, M., Liebmann, B., and Camilloni, I.: Influence of the South Atlantic
811 convergence zone and South Atlantic Sea surface temperature on interannual summer rainfall
812 variability in Southeastern South America, *Theoretical and Applied Climatology*, 67, 123–133,
813 2000.

814 Beck, H. E., van Dijk, A. I. J. M., Levizzani, V., Schellekens, J., Miralles, D. G., Martens, B., and
815 de Roo, A.: MSWEP: 3-hourly 0.25° global gridded precipitation (1979–2015) by merging
816 gauge, satellite, and reanalysis data, *Hydrology and Earth System Sciences*, 21, 589–615,
817 <https://doi.org/10.5194/hess-21-589-2017>, 2017.

818 Beck, H. E., Wood, E. F., Pan, M., Fisher, C. K., Miralles, D. G., Van Dijk, A. I., McVicar, T. R.,
819 and Adler, R. F.: MSWEP V2 global 3-hourly 0.1° precipitation: methodology and quantitative
820 assessment, *Bulletin of the American Meteorological Society*, 100, 473–500,
821 <https://doi.org/10.1175/BAMS-D-17-0138.1>, 2019.

822 Best, M. J., Pryor, M., Clark, D. B., Rooney, G. G., Essery, R. L. H., Ménard, C. B., Edwards, J.
823 M., Hendry, M. A., Porson, A., Gedney, N., Mercado, L. M., Sitch, S., Blyth, E., Boucher, O.,
824 Cox, P. M., Grimmond, C. S. B., and Harding, R. J.: The Joint UK Land Environment



- 825 Simulator (JULES), model description – Part 1: Energy and water fluxes, Geoscientific Model
826 Development, 4, 677–699, <https://doi.org/10.5194/gmd-4-677-2011>, 2011.
- 827 Van Beek, L. P. H., Wada, Y., and Bierkens, M. F.: Global monthly water stress: 1. Water balance
828 and water availability, Water Resources Research, 47,
829 <https://doi.org/10.1029/2010WR009791>, 2011.
- 830 Bierkens, M. F.: Global hydrology 2015: State, trends, and directions, Water Resources Research,
831 51, 4923–4947, <https://doi.org/10.1002/2015WR017173>, 2015.
- 832 Boening, C., Willis, J. K., Landerer, F. W., Nerem, R. S., and Fasullo, J.: The 2011 La Niña: So
833 strong, the oceans fell, Geophysical Research Letters, 39,
834 <https://doi.org/10.1029/2012GL053055>, 2012.
- 835 Bosilovich, M. G., Robertson, F. R., and Stackhouse, P. W.: El Niño–Related Tropical Land
836 Surface Water and Energy Response in MERRA-2, Journal of Climate, 33, 1155–1176,
837 <https://doi.org/10.1175/JCLI-D-19-0231.1>, 2020.
- 838 Boussetta, S., Balsamo, G., Arduini, G., Dutra, E., McNorton, J., Choulga, M., Agustí-Panareda,
839 A., Beljaars, A., Wedi, N., Muñoz-Sabater, J., and et al.: ECLand: The ECMWF Land Surface
840 Modelling System, Atmosphere, 12, 723, <https://doi.org/10.3390/atmos12060723>, 2021.
- 841 Budyko, M. I. and Miller, D. H.: Climate and life, Academic Press, 1974.
- 842 Cáceres, D., Marzeion, B., Malles, J. H., Gutknecht, B., Müller Schmied, H., and Döll, P.:
843 Assessing global water mass transfers from continents to oceans over the period 1948–2016,
844 Hydrology and Earth System Sciences, 24, 4831–4851, [https://doi.org/10.5194/hess-24-4831-](https://doi.org/10.5194/hess-24-4831-2020)
845 [2020](https://doi.org/10.5194/hess-24-4831-2020), 2020.
- 846 Chandanpurkar, H. A., Hamlington, B. D., and Reager, J. T.: Global terrestrial water storage
847 reconstruction using cyclostationary empirical orthogonal functions (1979–2020), Remote
848 Sensing, 14, 5677, <https://doi.org/10.3390/rs14225677>, 2022.



- 849 Chao, N., Luo, Z., Wang, Z., and Jin, T.: Retrieving groundwater depletion and drought in the
850 Tigris-Euphrates Basin between 2003 and 2015, *Groundwater*, 56, 770–782,
851 <https://doi.org/10.1111/gwat.12611>, 2018.
- 852 Cherenkova, E. A., Semenova, I. G., Kononova, N. K., and et al.: Droughts and dynamics of
853 synoptic processes in the south of the East European Plain at the beginning of the twenty-first
854 century, *Arid Ecosystems*, 5, 45–56, <https://doi.org/10.1134/S2079096115020055>, 2015.
- 855 Chimani, B., Auer, I., Prohom, M., Nadbath, M., Paul, A., and Rasol, D.: Data rescue in selected
856 countries in connection with the EUMETNET DARE activity, *Geoscience Data Journal*, 9,
857 187–200, <https://doi.org/10.1002/gdj3.143>, 2022.
- 858 Church, J. A., Clark, P. U., Cazenave, A., Gregory, J. M., Jevrejeva, S., Levermann, A., Merrifield,
859 M. A., Milne, G. A., Nerem, R. S., Nunn, P. D., and Payne, A. J.: *Sea level change*, Cambridge
860 University Press, 2013.
- 861 Clelland, A. A., Marshall, G. J., and Baxter, R.: Evaluating the performance of key ERA-Interim,
862 ERA5 and ERA5-Land climate variables across Siberia, *International Journal of Climatology*,
863 44, 2318–2342, <https://doi.org/10.1002/joc.8456>, 2024.
- 864 Compo, G. P., Whitaker, J. S., Sardeshmukh, P. D., Matsui, N., Allan, R. J., Yin, X., Gleason, B.
865 E., Vose, R. S., Rutledge, G., Bessemoulin, P., Brönnimann, S., Brunet, M., Crouthamel, R. I.,
866 Grant, A. N., Groisman, P. Y., Jones, P. D., Kruk, M. C., Kruger, A. C., Marshall, G. J.,
867 Maugeri, M., Mok, H. Y., Nordli, Ø., Ross, T. F., Trigo, R. M., Wang, X. L., Woodruff, S. D.,
868 and Worley, S. J.: The Twentieth Century Reanalysis Project, *Quarterly Journal of the Royal
869 Meteorological Society*, 137, 1–28, <https://doi.org/10.1002/qj.776>, 2011.
- 870 Costa, J. C., Verdán, I., Silva, M. E. S., Oscar-Júnior, A. C., and Ambrizzi, T.: South Atlantic
871 convergence zone and ENSO occurrence in the 2000–2021 period, *Theoretical and Applied
872 Climatology*, 155, 7079–7093, <https://doi.org/10.1007/s00704-024-04987-0>, 2024.
- 873 Cucchi, M., Weedon, G. P., Amici, A., Bellouin, N., Lange, S., Müller Schmied, H., Hersbach, H.,
874 and Buontempo, C.: WFDE5: bias-adjusted ERA5 reanalysis data for impact studies, *Earth
875 System Science Data*, 12, 2097–2120, <https://doi.org/10.5194/essd-12-2097-2020>, 2020.



- 876 Deng, S., Liu, Y., and Zhang, W.: A comprehensive evaluation of GRACE-like terrestrial water
877 storage (TWS) reconstruction products at an interannual scale during 1981–2019, *Water*
878 *Resources Research*, 59, e2022WR034381, <https://doi.org/10.1029/2022WR034381>, 2023.
- 879 Dharpure, J. K., Howat, I. M., and Kaushik, S.: Declining groundwater storage in the Indus basin
880 revealed using GRACE and GRACE-FO data, *Water Resources Research*, 61,
881 e2024WR038279, <https://doi.org/10.1029/2024WR038279>, 2025.
- 882 Diniz, F. L. and Todling, R.: Assessing the impact of observations in a multi-year reanalysis,
883 *Quarterly Journal of the Royal Meteorological Society*, 146, 724–747,
884 <https://doi.org/10.1002/qj.3705>, 2020.
- 885 Dutta, R. and Markonis, Y.: Does ERA5-land capture the changes in the terrestrial hydrological
886 cycle across the globe?, *Environmental Research Letters*, 19, 024054,
887 <https://doi.org/10.1088/1748-9326/ad1d3a>, 2024.
- 888 Ek, M. B., Mitchell, K. E., Lin, Y., Rogers, E., Grunmann, P., Koren, V., Gayno, G., and Tarpley,
889 J. D.: Implementation of Noah land surface model advances in the National Centers for
890 Environmental Prediction operational mesoscale Eta model, *Journal of Geophysical Research:*
891 *Atmospheres*, 108, 8851, <https://doi.org/10.1029/2002JD003296>, 2003.
- 892 Elias, E., Rango, A., Smith, R., Maxwell, C., Steele, C., and Havstad, K.: Climate change,
893 agriculture and water resources in the Southwestern United States, *Journal of Contemporary*
894 *Water Research & Education*, 158, 46–61, <https://doi.org/10.1111/j.1936-704X.2016.03218.x>,
895 2016.
- 896 Famiglietti, J. S., Cazenave, A., Eicker, A., Reager, J. T., Rodell, M., and Velicogna, I.: Satellites
897 provide the big picture, *Science*, 349, 684–685, 2015.
- 898 Flechtner, F., Reigber, C., Rummel, R., and Balmino, G.: Satellite gravimetry: a review of its
899 realization, *Surveys in Geophysics*, 42, 1029–1074, [https://doi.org/10.1007/s10712-021-](https://doi.org/10.1007/s10712-021-09658-0)
900 [09658-0](https://doi.org/10.1007/s10712-021-09658-0), 2021.
- 901 Frieler, K., Volkholz, J., Lange, S., Schewe, J., Mengel, M., del Rocio Rivas López, M., Otto, C.,
902 Reyer, C. P. O., Karger, D. N., Malle, J. T., Treu, S., Menz, C., Blanchard, J. L., Harrison, C.



- 903 S., Petrik, C. M., Eddy, T. D., Ortega-Cisneros, K., Novaglio, C., Rousseau, Y., Watson, R.
904 A., Stock, C., Liu, X., Heneghan, R., Tittensor, D., Maury, O., Büchner, M., Vogt, T., Wang,
905 T., Sun, F., Sauer, I. J., Koch, J., Vanderkelen, I., Jägermeyr, J., Müller, C., Rabin, S., Klar, J.,
906 Vega del Valle, I. D., Lasslop, G., Chadburn, S., Burke, E., Gallego-Sala, A., Smith, N., Chang,
907 J., Hantson, S., Burton, C., Gädeke, A., Li, F., Gosling, S. N., Müller Schmied, H., Hattermann,
908 F., Wang, J., Yao, F., Hickler, T., Marcé, R., Pierson, D., Thiery, W., Mercado-Bettín, D.,
909 Ladwig, R., Ayala-Zamora, A. I., Forrest, M., and Bechtold, M.: Scenario setup and forcing
910 data for impact model evaluation and impact attribution within the third round of the Inter-
911 Sectoral Impact Model Intercomparison Project (ISIMIP3a), Geoscientific Model
912 Development, 17, 1–51, <https://doi.org/10.5194/gmd-17-1-2024>, 2024.
- 913 Gelaro, R., McCarty, W., Suárez, M. J., Todling, R., Molod, A., Takacs, L., Randles, C. A.,
914 Darmenov, A., Bosilovich, M. G., Reichle, R., and Wargan, K.: The modern-era retrospective
915 analysis for research and applications, version 2 (MERRA-2), Journal of Climate, 30, 5419–
916 5454, <https://doi.org/10.1175/JCLI-D-16-0758.1>, 2017.
- 917 Gleeson, T., Cuthbert, M., Ferguson, G., and Perrone, D.: Global groundwater sustainability,
918 resources, and systems in the Anthropocene, Annual Review of Earth and Planetary Sciences,
919 48, 431–463, 2020.
- 920 Gleixner, S., Demissie, T., and Diro, G. T.: Did ERA5 improve temperature and precipitation
921 reanalysis over East Africa?, Atmosphere, 11, 996, <https://doi.org/10.3390/atmos11090996>,
922 2020.
- 923 Global SPEI database: <https://spei.csic.es/database.html>, 2018.
- 924 Gosling, S. N., Müller Schmied, H., Bradley, A., Burek, P., Chang, J., Ciais, P., Grillakis, M.,
925 Guillaumot, L., Hanasaki, N., Hartley, A., Huang, H., Kou-Giesbrecht, S., Koutroulis, A.,
926 Ostberg, S., Otta, K., Qi, W., Satoh, Y., Stacke, T., Zhu, Q., and Schewe, J.: ISIMIP3a
927 Simulation Data from the Global Water Sector (v1.6), ISIMIP Repository,
928 <https://doi.org/10.48364/ISIMIP.398165.6>, 2025.



929 Hacker, C. and Kusche, J.: How realistic are multi-decadal reconstructions of GRACE-like total
930 water storage anomalies?, *Journal of Hydrology*, 645, 132180,
931 <https://doi.org/10.1016/j.jhydrol.2024.132180>, 2024.

932 Hanasaki, N., Yoshikawa, S., Pokhrel, Y., and Kanae, S.: A global hydrological simulation to
933 specify the sources of water used by humans, *Hydrology and Earth System Sciences*, 22, 789–
934 817, <https://doi.org/10.5194/hess-22-789-2018>, 2018.

935 Here is your reference list reformatted in the standard Copernicus Publications / HESS (Hydrology
936 and Earth System Sciences) and EGU sphere house style. The references are arranged in
937 alphabetical order.

938

939 **References**

940 Harding, R., Best, M., Blyth, E., Hagemann, S., Kabat, P., Tallaksen, L. M., Warnaars, T., Wiberg,
941 D., Weedon, G. P., Lanen, H. V., and Ludwig, F.: WATCH: Current knowledge of the
942 terrestrial global water cycle, *Journal of Hydrometeorology*, 12, 1149–1156,
943 <https://doi.org/10.1175/JHM-D-11-024.1>, 2011.

944 Harris, I. C.: CRU JRA v2.0: A forcings dataset of gridded land surface blend of Climatic Research
945 Unit (CRU) and Japanese reanalysis (JRA) data; Jan. 1901 - Dec. 2018, Centre for
946 Environmental Data Analysis,
947 <https://catalogue.ceda.ac.uk/uuid/7f785c0e80aa4df2b39d068ce7351bbb>, 2022.

948 Hersbach, H., Bell, B., Berrisford, P., Hirahara, S., Horányi, A., Muñoz-Sabater, J., Nicolas, J.,
949 Peubey, C., Radu, R., Schepers, D., and Simmons, A.: The ERA5 global reanalysis, *Quarterly
950 Journal of the Royal Meteorological Society*, 146, 1999–2049, <https://doi.org/10.1002/qj.3803>,
951 2020.

952 Huffman, G. J., Adler, R. F., Behrangi, A., Bolvin, D. T., Nelkin, E. J., Gu, G., and Ehsani, M. R.:
953 The new version 3.2 Global Precipitation Climatology Project (GPCP) monthly and daily
954 precipitation products, *Journal of Climate*, 36, 7635–7655, [https://doi.org/10.1175/JCLI-D-23-
955 0123.1](https://doi.org/10.1175/JCLI-D-23-0123.1), 2023.



- 956 Humphrey, V., Gudmundsson, L., and Seneviratne, S. I.: A global reconstruction of climate-driven
957 subdecadal water storage variability, *Geophysical Research Letters*, 44, 2300–2309,
958 <https://doi.org/10.1002/2017GL072564>, 2017.
- 959 Humphrey, V. and Gudmundsson, L.: GRACE-REC: a reconstruction of climate-driven water
960 storage changes over the last century, *Earth System Science Data*, 11, 1153–1170,
961 <https://doi.org/10.5194/essd-11-1153-2019>, 2019.
- 962 Jacob, T., Wahr, J., Pfeffer, W. T., and Swenson, S.: Recent contributions of glaciers and ice caps
963 to sea level rise, *Nature*, 482, 514–518, <https://doi.org/10.1038/nature10847>, 2012.
- 964 Joodaki, G., Wahr, J., and Swenson, S.: Estimating the human contribution to groundwater
965 depletion in the Middle East, from GRACE data, land surface models, and well observations,
966 *Water Resources Research*, 50, 2679–2692, <https://doi.org/10.1002/2013WR014633>, 2014.
- 967 Kayano, M. T., Andreoli, R. V., and Ferreira de Souza, R. A.: Relations between ENSO and the
968 South Atlantic SST modes and their effects on the South American rainfall, *International*
969 *Journal of Climatology*, 33, 2008–2021, <https://doi.org/10.1002/joc.3569>, 2013.
- 970 Kim, H.: Global Soil Wetness Project Phase 3 Atmospheric Boundary Conditions (Experiment 1),
971 Data Integration and Analysis System (DIAS), <https://doi.org/10.20783/DIAS.501>, 2017.
- 972 Kobayashi, S., Ota, Y., Harada, Y., Ebata, A., Morimoto, M., Tsunematsu, N., Small, G., Harada,
973 K., Kamahori, C., Kusui, K., Togashi, K., Miyaoka, H., Takahashi, K., Maki, M., Shindo, H.,
974 Matsushita, N., Tanabe, N., Tsuyuki, T., Nishina, R., and Yabuki, H.: The JRA-55 Reanalysis:
975 General Specifications and Basic Characteristics, *Journal of the Meteorological Society of*
976 *Japan*, 93, 5–48, <https://doi.org/10.2151/jmsj.2015-001>, 2015.
- 977 Landerer, F. W., Flechtner, F. M., Save, H., Webb, F. H., Bandikova, T., Bertiger, W. I., Burgess,
978 D. N., Doll, P., Watkins, M. M., and Wiese, D. N.: Extending the Global Mass Change Data
979 Record: GRACE Follow-On Instrument and Science Data Performance, *Geophysical Research*
980 *Letters*, 47, e2020GL088306, <https://doi.org/10.1029/2020GL088306>, 2020.



- 981 Li, B., Rodell, M., Sheffield, J., Wood, E. F., Wada, Y., and Gutmann, E.: Long-term, non-
982 anthropogenic groundwater storage changes simulated by three global-scale hydrological
983 models, *Scientific Reports*, 9, 10746, <https://doi.org/10.1038/s41598-019-47219-z>, 2019.
- 984 Li, F., Kusche, J., Chao, N., Wang, Z., and Löcher, A.: Long-term (1979-present) total water
985 storage anomalies over the global land derived by reconstructing GRACE data, *Geophysical
986 Research Letters*, 48, e2021GL093492, <https://doi.org/10.1029/2021GL093492>, 2021.
- 987 Liu, J., Hagan, D. F. T., and Liu, Y.: Global land surface temperature change (2003–2017) and its
988 relationship with climate drivers: AIRS, MODIS, and ERA5-land based analysis, *Remote
989 Sensing*, 13, 44, <https://doi.org/10.3390/rs13010044>, 2020.
- 990 Löcher, A. and Kusche, J.: A hybrid approach for recovering high-resolution temporal gravity
991 fields from satellite laser ranging, *Journal of Geodesy*, 95, 6, [https://doi.org/10.1007/s00190-
992 020-01460-x](https://doi.org/10.1007/s00190-020-01460-x), 2021.
- 993 Loomis, B. D., Luthcke, S. B., and Sabaka, T. J.: Regularization and error characterization of
994 GRACE mascons, *Journal of Geodesy*, 93, 1381–1398, [https://doi.org/10.1007/s00190-019-
995 01252-y](https://doi.org/10.1007/s00190-019-01252-y), 2019a.
- 996 Loomis, B. D., Rachlin, K. E., and Luthcke, S. B.: Improved Earth oblateness rate reveals increased
997 ice sheet losses and mass-driven sea level rise, *Geophysical Research Letters*, 46, 6910–6917,
998 <https://doi.org/10.1029/2019GL082929>, 2019b.
- 999 Maidment, R. I., Allan, R. P., and Black, E.: Recent observed and simulated changes in
1000 precipitation over Africa, *Geophysical Research Letters*, 42, 8155–8164,
1001 <https://doi.org/10.1002/2015GL065765>, 2015.
- 1002 Marengo, J. A., Torres, R. R., and Alves, L. M.: Drought in Northeast Brazil—past, present, and
1003 future, *Theoretical and Applied Climatology*, 129, 1189–1200,
1004 <https://doi.org/10.1007/s00704-016-1985-y>, 2017.
- 1005 Miralles, D. G., Van Den Berg, M. J., Gash, J. H., Parinussa, R. M., De Jeu, R. A., Beck, H. E.,
1006 Holmes, T. R., Jiménez, C., Verhoest, N. E., Dorigo, W. A., and Teuling, A. J.: El Niño–La



- 1007 Niña cycle and recent trends in continental evaporation, *Nature Climate Change*, 4, 122–126,
1008 <https://doi.org/10.1038/nclimate2068>, 2014.
- 1009 Müller Schmied, H., Trautmann, T., Ackermann, S., Cáceres, D., Flörke, M., Gerdener, H.,
1010 Kynast, E., Asali Peiris, T., Schiebener, L., Schumacher, M., and Döll, P.: The global water
1011 resources and use model WaterGAP v2.2e, *Geoscientific Model Development*, 17, 3011–3043,
1012 <https://doi.org/10.5194/gmd-16-3011-2023>, 2023.
- 1013 Muñoz-Sabater, J., Dutra, E., Agustí-Panareda, A., Albergel, C., Arduini, G., Balsamo, G.,
1014 Bousssetta, S., Choulga, M., Harrigan, S., Hersbach, H., Martens, B., Miralles, D. G., Piles, M.,
1015 Rodríguez-Fernández, N. J., Zsoter, E., Buontempo, C., and Thépaut, J.-N.: ERA5-Land: a
1016 state-of-the-art global reanalysis dataset for land applications, *Earth System Science Data*, 13,
1017 4349–4383, <https://doi.org/10.5194/essd-13-4349-2021>, 2021.
- 1018 Nicholson, S. E.: Spatial teleconnections in African rainfall: A comparison of 19th and 20th
1019 century patterns, *The Holocene*, 24, 1840–1848, <https://doi.org/10.1177/0959683614551230>,
1020 2014.
- 1021 Nicholson, S. E., Klotter, D., Dezfuli, A. K., and Zhou, L.: New rainfall datasets for the Congo
1022 Basin and surrounding regions, *Journal of Hydrometeorology*, 19, 1379–1396,
1023 <https://doi.org/10.1175/JHM-D-18-0051.1>, 2018.
- 1024 Ni, S., Chen, J., Wilson, C. R., and Li, J.: Global Terrestrial Water Storage Changes and
1025 Connections to ENSO Events, *Surveys in Geophysics*, 39, 1–22,
1026 <https://doi.org/10.1007/s10712-017-9421-7>, 2018.
- 1027 Nie, Y., Chen, J., Xu, G., and Löcher, A.: Barystatic sea level change observed by satellite
1028 gravimetry: 1993–2022, *Proceedings of the National Academy of Sciences*, 122,
1029 e2425248122, <https://doi.org/10.1073/pnas.2425248122>, 2025.
- 1030 Nobre, P. and Shukla, J.: Variations of sea surface temperature, wind stress, and rainfall over the
1031 tropical Atlantic and South America, *Journal of Climate*, 9, 2464–2479,
1032 [https://doi.org/10.1175/1520-0442\(1996\)009<2464:VOSSTW>2.0.CO;2](https://doi.org/10.1175/1520-0442(1996)009<2464:VOSSTW>2.0.CO;2), 1996.



- 1033 Nogueira, M.: Inter-comparison of ERA-5, ERA-interim and GPCP rainfall over the last 40 years:
1034 Process-based analysis of systematic and random differences, *Journal of Hydrology*, 583,
1035 124632, <https://doi.org/10.1016/j.jhydrol.2020.124632>, 2020.
- 1036 Oki, T. and Sud, Y. C.: Design of Total Runoff Integrating Pathways (TRIP)—A Global River
1037 Channel Network, *Earth Interactions*, 2, 1–37, [https://doi.org/10.1175/1087-3562\(1998\)002<0001:DOTRIP>2.3.CO;2](https://doi.org/10.1175/1087-3562(1998)002<0001:DOTRIP>2.3.CO;2), 1998.
- 1039 Palmer, W. C.: Meteorological drought, U.S. Department of Commerce, Washington, D. C.,
1040 Research Paper No. 45, 58 pp., 1965.
- 1041 Phillips, T., Nerem, R. S., Fox-Kemper, B., Famiglietti, J. S., and Rajagopalan, B.: The influence
1042 of ENSO on global terrestrial water storage using GRACE, *Geophysical Research Letters*, 39,
1043 <https://doi.org/10.1029/2012GL052495>, 2012.
- 1044 Pokhrel, Y. N., Hanasaki, N., Yeh, P.-J. F., Döll, P., Kanai, S., and Oki, T.: Model estimates of
1045 sea-level change due to anthropogenic impacts on terrestrial water storage, *Nature Geoscience*,
1046 5, 389–392, <https://doi.org/10.1038/ngeo1476>, 2012.
- 1047 Reichle, R. H.: The MERRA-land data product, NASA Goddard Modeling and Assimilation
1048 Office, Technical Report Series, GMAO Office Note 3, Version 1.2, 38 pp., 2012.
- 1049 Robertson, F. R., Bosilovich, M. G., and Roberts, J. B.: Reconciling land–
1050 ocean moisture transport variability in reanalyses with P–E in
1051 observationally driven land surface models, *Journal of Climate*, 29,
1052 8625–8646, <https://doi.org/10.1175/JCLI-D-16-0175.1>, 2016.
- 1053 Rodell, M., Barnoud, A., Robertson, F. R., Famiglietti, J. S., Reager, J. T., and Lombard, A.: An
1054 Abrupt Decline in Global Terrestrial Water Storage and Its Relationship with Sea Level
1055 Change, *Surveys in Geophysics*, 45, 1875–1902, <https://doi.org/10.1007/s10712-024-09860-w>, 2024.
- 1057 Rodell, M., Houser, P. R., Jambor, U., Gottschalck, J., Mitchell, K., Meng, C.-J., Arsenault, K.,
1058 Cosgrove, B., Radakovich, J., Bosilovich, M., Entin, J. K., Walker, J. P., Lohmann, D., and



- 1059 Toll, D.: The Global Land Data Assimilation System, *Bulletin of the American Meteorological*
1060 *Society*, 85, 381–394, <https://doi.org/10.1175/BAMS-85-3-381>, 2004.
- 1061 Rodell, M., Famiglietti, J. S., Wiese, D. N., Reager, J. T., Beaudoing, H. K., Landerer, F. W., and
1062 Scanlon, B. R.: Emerging trends in global freshwater availability, *Nature*, 557, 651–659,
1063 <https://doi.org/10.1038/s41586-018-0123-1>, 2018.
- 1064 Rodell, M. and Reager, J. T.: Water cycle science enabled by the GRACE and GRACE-FO satellite
1065 missions, *Nature Water*, 1, 47–59, <https://doi.org/10.1038/s44221-022-00005-0>, 2023.
- 1066 Rodell, M., Velicogna, I., and Famiglietti, J. S.: Satellite-based estimates of groundwater depletion
1067 in India, *Nature*, 460, 999–1002, <https://doi.org/10.1038/nature08238>, 2009.
- 1068 Rosenzweig, C., Arnell, N. W., Ebi, K. L., Lotze-Campen, H., Raes, F., Rapley, C., Smith, M. S.,
1069 Cramer, W., Frieler, K., Reyer, C. P., and Schewe, J.: Assessing inter-sectoral climate change
1070 risks: the role of ISIMIP, *Environmental Research Letters*, 12, 010301,
1071 <https://doi.org/10.1088/1748-9326/12/1/010301>, 2017.
- 1072 Rowlands, D. D., Luthcke, S. B., Klosko, S. M., Lemoine, F. G. R., Chinn, D. S., McCarthy, J. J.,
1073 Cox, C. M., and Anderson, O. B.: Resolving mass flux at high spatial and temporal resolution
1074 using GRACE intersatellite measurements, *Geophysical Research Letters*, 32, L04310,
1075 <https://doi.org/10.1029/2004GL021509>, 2005.
- 1076 Here is your reference list reformatted in the standard Copernicus Publications / HESS (Hydrology
1077 and Earth System Sciences) and EGU sphere house style. The references are arranged in
1078 alphabetical order.

1079

1080 References

- 1081 Save, H., Bettadpur, S., and Tapley, B. D.: High resolution CSR GRACE RL05 mascons, *Journal*
1082 *of Geophysical Research: Solid Earth*, 121, <https://doi.org/10.1002/2016JB013007>, 2016.
- 1083 Scanlon, B.R., Zhang, Z., Save, H., Sun, A.Y., Müller Schmied, H., Van Beek, L.P., Wiese, D.N.,
1084 Wada, Y., Long, D., Reedy, R.C. and Longuevergne, L., 2018. Global models underestimate



1085 large decadal declining and rising water storage trends relative to GRACE satellite data.
1086 Proceedings of the National Academy of Sciences, 115(6), pp.E1080-
1087 E1089. <https://doi.org/10.1073/pnas.1704665115>, 2018.

1088 Scanlon, B. R., Fakhreddine, S., Rateb, A., de Graaf, I., Famiglietti, J., Gleeson, T., Grafton, R.
1089 Q., Jobbagy, E., Kebede, S., Kolusu, S. R., and Konikow, L. F.: Global water resources and
1090 the role of groundwater in a resilient water future, *Nature Reviews Earth & Environment*, 4,
1091 87–101, <https://doi.org/10.1038/s43017-022-00382-w>, 2023.

1092 Selva, D., Golkar, A., Korobova, O., Cruz, I. L. I., Collopy, P., and de Weck, O. L.: Distributed
1093 earth satellite systems: What is needed to move forward?, *Journal of Aerospace Information*
1094 *Systems*, 14, 412–438, <https://doi.org/10.2514/1.I010531>, 2017.

1095 Semenova, I. and Vicente-Serrano, S. M.: Long-term variability and trends of meteorological
1096 droughts in Ukraine, *International Journal of Climatology*, 44, 1849–1866,
1097 <https://doi.org/10.1002/joc.8416>, 2024.

1098 Semenova, I. and Slizhe, M.: Synoptic conditions of droughts and dry winds in the Black Sea
1099 Steppe Province under recent decades, *Frontiers in Earth Science*, 8, 69,
1100 <https://doi.org/10.3389/feart.2020.00069>, 2020.

1101 Sheffield, J. and Wood, E. F.: Characteristics of global and regional drought, 1950–2000: Analysis
1102 of soil moisture data from off-line simulation of the terrestrial hydrologic cycle, *Journal of*
1103 *Geophysical Research: Atmospheres*, 112, D17101, <https://doi.org/10.1029/2006JD008288>,
1104 2007.

1105 Sitch, S., Smith, B., Prentice, I. C., Arneth, A., Bondeau, A., Cramer, W., Kaplan, J. O., Levis, S.,
1106 Lucht, W., Sykes, M. T., Thonicke, K., and Venevsky, S.: Evaluation of ecosystem dynamics,
1107 plant geography and terrestrial carbon cycling in the LPJ dynamic global vegetation model,
1108 *Global Change Biology*, 9, 161–185, <https://doi.org/10.1046/j.1365-2486.2003.00569.x>, 2003.

1109 Slivinski, L. C., Compo, G. P., Whitaker, J. S., Sardeshmukh, P. D., Giese, B. S., McColl, C.,
1110 Allan, R. J., Yin, X., Vose, R., Titchner, H., Kennedy, J., Broccoli, A. J., Camargo, S. J.,
1111 Chemke, J., A., K., Compo, G. P., Cowan, T., Crouthamel, R. I., Feng, S., Groisman, P. Y.,



- 1112 Hoell, A., Kruger, A. C., Lazante, J. R., Lemke, P., Lorant, M. M., McVicar, T. R., Misra,
1113 V., Morse, A. P., Murphy, S., Palecki, M., Rodell, M., Rutledge, G., Schreiber, S. L., Slivinski,
1114 A. B., Smith, A. J., Thorne, P. W., Valente, M. A., Vautard, R., Wang, X. L., Woodruff, S. D.,
1115 and Worley, S. J.: Towards a more reliable historical reanalysis: Improvements for version 3
1116 of the Twentieth Century Reanalysis system, *Quarterly Journal of the Royal Meteorological*
1117 *Society*, 145, 2876–2908, <https://doi.org/10.1002/qj.3598>, 2019.
- 1118 Sośnica, K., Jäggi, A., Meyer, U., Thaller, D., Beutler, G., and Dach, R.: Time variable Earth's
1119 gravity field from SLR satellites, *Journal of Geodesy*, 89, 945–960,
1120 <https://doi.org/10.1007/s00190-015-0825-1>, 2015.
- 1121 de Souza Santos, J. A., Wanderley, H. S., de Amorim, R. F. C., Delgado, R. C., and Fernandes, R.
1122 C.: The longest multiannual drought in Northeastern Brazil, *Journal of South American Earth*
1123 *Sciences*, 143, 104976, <https://doi.org/10.1016/j.jsames.2024.104976>, 2024.
- 1124 Su, J., Miao, C., Zwiers, F., Sheffield, J., and Zhang, X.: Precipitation observing network gaps
1125 limit climate change impact assessment, *Nature*, 652, 119–125,
1126 <https://doi.org/10.1038/s41586-026-10300-5>, 2026.
- 1127 Tapley, B. D., Watkins, M. M., Flechtner, F., Reigber, C., Bettadpur, S., and Rodell, M.:
1128 Contributions of GRACE to understanding climate change, *Nature Climate Change*, 9, 358–
1129 369, <https://doi.org/10.1038/s41558-019-0456-2>, 2019.
- 1130 Telteu, C.-E., Müller Schmied, H., Thiery, W., Leng, G., Burek, P., Liu, X., Boulange, J. E. S.,
1131 Andersen, L. S., Grillakis, M., Gosling, S. N., Satoh, Y., Rakovec, O., Stacke, T., Chang, J.,
1132 Wanders, N., Shah, H. L., Trautmann, T., Mao, G., Hanasaki, N., Koutroulis, A., Pokhrel, Y.,
1133 Samaniego, L., Wada, Y., Mishra, V., Liu, J., Döll, P., Zhao, F., Gädeke, A., Rabin, S. S., and
1134 Herz, F.: Understanding each other's models: an introduction and a standard representation of
1135 16 global water models to support intercomparison, improvement, and communication,
1136 *Geoscientific Model Development*, 14, 3843–3878, [https://doi.org/10.5194/gmd-14-3843-](https://doi.org/10.5194/gmd-14-3843-2021)
1137 [2021](https://doi.org/10.5194/gmd-14-3843-2021), 2021.
- 1138 Thorne, P. W., Allan, R. J., Ashcroft, L., Brohan, P., Dunn, R. H., Menne, M. J., Pearce, P. R.,
1139 Picas, J., Willett, K. M., Benoy, M., and Brönnimann, S.: Toward an integrated set of surface



- 1140 meteorological observations for climate science and applications, *Bulletin of the American*
1141 *Meteorological Society*, 98, 2689–2702, <https://doi.org/10.1175/BAMS-D-16-0165.1>, 2017.
- 1142 Tiwari, A. D., Pokhrel, Y., Boulange, J., Felfelani, F., Wada, Y., Müller Schmied, H., Hanasaki,
1143 N., Burek, P., and Satoh, Y.: Similarities and divergent patterns in hydrologic fluxes and
1144 storages simulated by global water models, *Nature Water*, 3, 550–560,
1145 <https://doi.org/10.1038/s44221-025-00435-6>, 2025.
- 1146 Trenberth, K. E. and Shea, D. J.: Relationships between precipitation and surface temperature,
1147 *Geophysical Research Letters*, 32, L14703, <https://doi.org/10.1029/2005GL022760>, 2005.
- 1148 Van Beek, L. P. H., Wada, Y., and Bierkens, M. F.: Global monthly water stress: 1. Water balance
1149 and water availability, *Water Resources Research*, 47,
1150 <https://doi.org/10.1029/2010WR009791>, 2011.
- 1151 Vörösmarty, C. J., Green, P., Salisbury, J., and Lammers, R. B.: Global water resources:
1152 Vulnerability from climate change and population growth, *Science*, 289, 284–288,
1153 <https://doi.org/10.1126/science.289.5477.284>, 2000.
- 1154 Velicogna, I., Sutterley, T. C., and Van Den Broeke, M. R.: Regional acceleration in ice mass loss
1155 from Greenland and Antarctica using GRACE time-variable gravity data, *Geophysical*
1156 *Research Letters*, 41, 8130–8137, <https://doi.org/10.1002/2014GL061052>, 2014.
- 1157 Velicogna, I., Mohajerani, Y., A, G., Landerer, F., Mouginot, J., Noel, B., Rignot, E., Sutterley,
1158 T., van den Broeke, M., van Wessum, M., and Wiese, D.: Continuity of ice sheet mass loss in
1159 Greenland and Antarctica from the GRACE and GRACE follow-on missions, *Geophysical*
1160 *Research Letters*, 47, e2020GL087291, <https://doi.org/10.1029/2020GL087291>, 2020.
- 1161 Wada, Y., Bierkens, M. F. P., de Roo, A., Dirmeyer, P. A., Famiglietti, J. S., Hanasaki, N., Konar,
1162 M., Liu, J., Müller Schmied, H., Oki, T., Pokhrel, Y., Sivapalan, M., Troy, T. J., van Dijk, A.
1163 I. J. M., van Emmerik, T., Van Huijgevoort, M. H. J., Van Lanen, H. A. J., Vörösmarty, C. J.,
1164 Wanders, N., and Wheeler, H.: Human–water interface in hydrological modelling: current
1165 status and future directions, *Hydrology and Earth System Sciences*, 21, 4169–4193,
1166 <https://doi.org/10.5194/hess-21-4169-2017>, 2017.



- 1167 Wada, Y., Wisser, D., and Bierkens, M. F. P.: Global modeling of withdrawal, allocation and
1168 consumptive use of surface water and groundwater resources, *Earth System Dynamics*, 5, 15–
1169 40, <https://doi.org/10.5194/esd-5-15-2014>, 2014.
- 1170 Wada, Y., Van Beek, L. P., Van Kempen, C. M., Reckman, J. W., Vasak, S., and Bierkens, M. F.:
1171 Global depletion of groundwater resources, *Geophysical Research Letters*, 37,
1172 <https://doi.org/10.1029/2010GL044571>, 2010.
- 1173 Wainwright, C. M., Allan, R. P., and Black, E.: Consistent trends in dry spell length in recent
1174 observations and future projections, *Geophysical Research Letters*, 49, e2021GL097231,
1175 <https://doi.org/10.1029/2021GL097231>, 2022.
- 1176 Wang, W., Feng, S., Zhang, Y., Wei, Z., Dong, J., Weihermüller, L., Liu, C.-Q., and Vereecken,
1177 H.: Fusing ERA5-Land and SMAP L4 for an improved global soil moisture product (1950–
1178 2025), *Earth System Science Data*, 18, 1061–1088, [https://doi.org/10.5194/essd-18-1061-](https://doi.org/10.5194/essd-18-1061-2026)
1179 [2026](https://doi.org/10.5194/essd-18-1061-2026), 2026.
- 1180 Wang, Y.-R., Hessen, D. O., Samset, B. H., and Stordal, F.: Evaluating global and regional land
1181 warming trends in the past decades with both MODIS and ERA5-Land land surface
1182 temperature data, *Remote Sensing of Environment*, 280, 113181,
1183 <https://doi.org/10.1016/j.rse.2022.113181>, 2022.
- 1184 Warszawski, L., Frieler, K., Huber, V., Piontek, O., Serdeczny, O., and Schewe, J.: The Inter-
1185 Sectoral Impact Model Intercomparison Project (ISI-MIP): Project framework, *Proceedings*
1186 *of the National Academy of Sciences of the United States of America*, 111, 3228–3232,
1187 <https://doi.org/10.1073/pnas.1312330110>, 2014.
- 1188 Washington, R., James, R., Pearce, H., Pokam, W. M., and Moufouma-Okia, W.: Congo Basin
1189 rainfall climatology: can we believe the climate models?, *Philosophical Transactions of the*
1190 *Royal Society B: Biological Sciences*, 368, 20120296, <https://doi.org/10.1098/rstb.2012.0296>,
1191 2013.
- 1192 Weedon, G. P., Gomes, S., Viterbo, P., Shuttleworth, W. J., Blyth, E., Österle, H., Adam, J. C.,
1193 Bellouin, N., Boucher, O., and Best, M.: Creation of the WATCH Forcing Data and Its Use to



- 1194 Assess Global and Regional Reference Crop Evaporation over Land during the Twentieth
1195 Century, *Journal of Hydrometeorology*, 12, 823–848,
1196 <https://doi.org/10.1175/2011JHM1369.1>, 2011.
- 1197 Weedon, G. P., Balsamo, G., Bellouin, N., Gomes, S., Best, M. J., and Viterbo, P.: The WFDEI
1198 meteorological forcing data set: WATCH Forcing Data methodology applied to ERA-Interim
1199 reanalysis data, *Water Resources Research*, 50, 7505–7514,
1200 <https://doi.org/10.1002/2014WR015638>, 2014.
- 1201 Wiese, D. N., Yuan, D.-N., Boening, C., Landerer, F. W., and Watkins, M. M.: JPL GRACE
1202 Mascon Ocean, Ice, and Hydrology Equivalent Water Height Release 06 Coastal Resolution
1203 Improvement (CRI) Filtered Version 1.0, PO.DAAC, California,
1204 <https://doi.org/10.5067/TEMSC-3MJC6>, 2018.
- 1205 Wirth, S. B., Braun, J., Heinke, J., Ostberg, S., Rolinski, S., Schaphoff, S., Stenzel, F., von Bloh,
1206 W., Taube, F., and Müller, C.: Biological nitrogen fixation of natural and agricultural
1207 vegetation simulated with LPJmL 5.7.9, *Geoscientific Model Development*, 17, 7889–7914,
1208 <https://doi.org/10.5194/gmd-17-7889-2024>, 2024.
- 1209 Wu, Z. and Huang, N. E.: Ensemble Empirical Mode Decomposition: A Noise-Assisted Data
1210 Analysis Method, *Advances in Adaptive Data Analysis*, 1, 1–41,
1211 <https://doi.org/10.1142/S1793536909000047>, 2009.
- 1212 Yin, J., Slater, L. J., Khouakhi, A., Yu, L., Liu, P., Li, F., Pokhrel, Y., and Gentine, P.: GTWS-
1213 MLrec: global terrestrial water storage reconstruction by machine learning from 1940 to
1214 present, *Earth System Science Data*, 15, 5597–5615, [https://doi.org/10.5194/essd-15-5597-](https://doi.org/10.5194/essd-15-5597-2023)
1215 [2023](https://doi.org/10.5194/essd-15-5597-2023), 2023.
- 1216 Zhang, Y., He, B., Guo, L., Liu, J., and Xie, X.: The relative contributions of precipitation,
1217 evapotranspiration, and runoff to terrestrial water storage changes across 168 river basins,
1218 *Journal of Hydrology*, 579, 124194, <https://doi.org/10.1016/j.jhydrol.2019.124194>, 2019.